Achromobacter xylosoxidans isolates exhibit genome diversity, variable virulence, high levels of antibiotic resistance and potential intrahost evolution.

Pooja Acharya[1], Cameron Lloyd[1], Jessica Kumke[1], Zilia Yanira Muñoz Ramirez[2], and Hanh Ngoc Lam[1]

[1] Department of Biological Sciences, Virginia Tech, 970 Washington Street NW, Blacksburg, VA 24061, USA

[2] Facultad de Ciencias Químicas, Universidad Autónoma de Chihuahua, Campus II Circuito Universitario s/n, Chihuahua 31125, Mexico

Corresponding author and email address

Hanh Ngoc Lam, hanhlam@vt.edu

Abstract

Achromobacter xylosoxidans is an emerging pathogen characterized by high levels of antibiotic resistance and increasing infection rates worldwide. This motile, opportunistic pathogen is widely distributed in the environment and can cause various infections, including pneumonia, bacteremia, endocarditis, meningitis, and others. In this study, we analyzed the population structure, antibiotic resistance profiles, and virulence factors of over 200 publicly available genomes. Core genome analysis revealed that *A. xylosoxidans* is highly adaptable, possessing a relatively small core genome. Antibiotic susceptibility testing of isolates from the United States revealed high resistance to multiple antibiotics including ceftolozane/tazobactam, aztreonam, cefepime, and ciprofloxacin. Our data show that imipenem/relebactam (IMR) is not more effective against *A. xylosoxidans* than imipenem (IMI) alone, indicating that relebactam does not inhibit β-lactamase activity in Achromobacter. The species features multiple secretion systems, including the Type III secretion system (T3SS) of the YscN family, which is similar to those found in *Bordetella pertussis* and *Pseudomonas aeruginosa*. Isolates collected from the same patients showed dynamic changes in cytotoxicity, flagella motility, biofilm and antibiotic resistance suggesting its dynamic adaptation to host environment. Intra-host evolved isolates, NIH-010 and NIH-016, demonstrated the loss of flagella motility and variable cytotoxicity while exhibiting increased antibiotic resistance and enhanced biofilm formation. Sequence analysis suggests that NIH-016-3 has tyrosine to histidine mutation at position 330 (Y330H) near the FlhF Guanosine triphosphate (GTP)-binding domain that may affect flagellar assembly. Interestingly, virulence assays showed significant variation in the ability of different *A. xylosoxidans* isolates to induce

cell death in *in vitro* models, suggesting its dynamic adaptation to host environment. These findings highlight the complexity of this pathogen group and underscore the urgent need for further research into its mechanisms of antibiotic resistance and virulence.

Impact statement

This study provides a comprehensive examination of *Achromobacter xylosoxidans*, an emerging pathogen of global concern due to its high antibiotic resistance and increasing clinical relevance. By analyzing over 200 genomes, we offer critical insights into the population structure, resistance mechanisms, and virulence factors of this species. The identification of a relatively small core genome underscores the adaptability of *A. xylosoxidans* and its potential for genomic plasticity. The existence of multiple secretion systems (T1SS to T6SS) highlights the great capacity of *A. xylosoxidans* as a pathogen. Variations in virulence among *A. xylosoxidans* isolates indicate the complexity of this pathogen and underscore the need for further studies on its virulence mechanisms. The dynamic within-host evolution including the loss of motility-associated systems and the acquisition of enhanced antibiotic resistance and biofilm formation, adds new dimensions to our understanding of its pathogenesis. Flagella, an important virulence mechanism, exhibit variable motility in different isolates, suggesting the bacteria use flagella as an adaptive mechanism. This work also showed that *A. xylosoxidans* are resistant to relebactam, which are effective in other bacteria. These findings emphasize the urgent need for targeted therapeutic strategies to combat this opportunistic pathogen.

1. Introduction

The genus *Achromobacter* is a non-lactose fermenting, Gram-negative, motile bacterium recognized as an emerging pathogen in cystic fibrosis (CF) patients (1). It belongs to the β-proteobacteria class. While *Achromobacter* species are ubiquitously found in water and soil, and can grow in the plant rhizosphere, *A. xylosoxidans* isolates are primarily clinically derived (2). This bacterium was first isolated in 1971 from an ear infection (3). *A. xylosoxidans* can cause a wide range of infections, including pneumonia, bacteremia, endocarditis, meningitis, and others (4, 5). These infections, which predominantly affect immunocompromised individuals often lead to severe outcomes (4). Colonization with *A. xylosoxidans* is considered a marker of disease severity in CF patients (6) and is associated with a decline in respiratory function (7) and with a greater risk of death in lung transplant recipients (8). The persistence of *A. xylosoxidans* in both extreme environments and host organisms may be attributed to its genetic diversity and adaptability, although this aspect remains poorly understood (9). Earlier studies examining the genomic diversity of this bacterial genus across six genomes revealed a

74 higher percentage of accessory genes in *Achromobacter spp*. (10). Recent virulence studies
75 have utilized various clinical isolates to explore its pathogenic mechanisms (11-13). As of the
76 time of this study, nearly 200 genomes of *A. xylosoxidans* were available on NCBI. However,
77 comprehensive analyses of the differences among isolates with respect to their genomic
78 content, virulence potential, and antibiotic resistance profiles are lacking.

79

80 Clinical isolates possess unique genomic features that differentiate them from environmental
81 isolates and contribute to virulence, such as the type III secretion system (T3SS), a
82 polysaccharide island, adhesion-related proteins, and several putative toxins (14). In addition
83 to these genetic elements, the Type VI Secretion System (T6SS) has been recently identified
84 to contribute to virulence alongside the T3SS (15, 16). The T3SS enables bacteria to deliver
85 effector proteins directly into the cytosol of animal or plant host cells. These systems have
86 diversified into seven families, spreading across Gram-negative bacteria through horizontal
87 gene transfer (17). The T6SS facilitates bacterial competition and functions as a virulence
88 factor in various pathogenic bacteria (18, 19). In *A. xylosoxidans*, the activity of the T6SS
89 contributes to the internalization in immune cells wherein it expresses cytotoxic effectors (12,
90 19). Some environmental isolates also contain phage regions encoding components of type IV
91 secretion systems (T4SS), and several genetic islands that may enhance survival in host-free
92 environments (10). In addition to secretion systems, motility is a major virulence factor in
93 pathogenic bacteria with *A. xylosoxidans* producing peritrichous flagella (20). Loss of
94 functional flagella is commonly associated with reduced virulence (21).

95 The genus *Achromobacter* is well-known for its inherent resistance to a broad range of
96 antimicrobial agents (22) and its ability to acquire resistance to commonly used treatments
97 for respiratory infections, such as colistin and carbapenems (22, 23). *A. xylosoxidans* encodes
98 at least 50 drug resistance – associated genes, including β-lactamases, efflux pumps, and
99 transposons (24). Seventeen different efflux pumps have been identified in *A. xylosoxidans,*
100 which may contribute to its intrinsic resistance (24). However, to date, only three of these
101 efflux pumps have been characterized. Notably, the observed susceptibility profiles often
102 poorly correlate with the presence of putative resistance genes (24). These findings
103 highlight the need to investigate the prevalence and mechanisms of antibiotic resistance
104 (AR) among *A. xylosoxidans* isolates. A powerful tool for the investigation of bacterial
105 genomics is supervised machine learning (ML). Supervised ML has been implemented to
106 identify the resistance profiles of multiple organisms based on genomic characteristics alone
107 (25). Usage of this technique therefore enables the prediction of antimicrobial resistance
108 and the identification of potential resistance genes across *A. xylosoxidans* isolates (26-29).

109 Biofilm formation can contribute significantly to antibiotic resistance, as the biofilm matrix
110 provides a protective environment that limits antibiotic penetration and promotes the survival
111 of persistent cells (30). Additionally, motility structures such as flagella may play a role in the
112 initial attachment and establishment of biofilms. *A. xylosoxidans* appeared to downregulate
113 its flagellar gene expression during biofilm formation (31).

114 In this work, we examined the genomic diversity of all available genome sequences of *A.*
115 *xylosoxidans*. Phylogenetic analysis was performed on a total of 178 genomes, including those
116 from NCBI and our recently collected clinical isolates from the NIH clinical center. Given the
117 critical role of secretion systems and motility in virulence, we analyzed the presence of all
118 secretion systems (types I to IX) and flagellar system in our NIH clinical isolates. Phylogenetic
119 analysis was further used to classify the T3SS family of *A. xylosoxidans*. We used our previously
120 collected whole genome sequences and susceptibility testing data from the clinical isolates to
121 predict AR among NCBI genomes using machine learning. The cytotoxicity, biofilm and motility
122 were assayed.

123

124 ## 2. Methods

125

126 **Data used in this work:**

127 Raw sequence data from Bio Project ID PRJNA1148967, referred to as NIH data with 38
128 *Achromobacter xylosoxidans*, *A. denitrificans, A. ruhlandii, A. mucicolens and A. insolitus*
129 genomes. 197 genomes of *Achromobacter xylosoxidans* from NCBI
130 (https://www.ncbi.nlm.nih.gov/datasets/genome/?taxon=85698&assembly_level=1:3) as of
131 September 2024, referred as NCBI data.

132

133 **Genome assembly**

134 For all NIH isolates: Adapters were trimmed using Trimmomatic version V0.39 (32) with
135 default parameters, except the last 10 bases were removed. FastQC (v0.11.9) (33) was used
136 to visualize read quality, which showed an average base sequence quality greater than 28
137 across the reads. Genome assembly was performed using SPAdes (34) in careful mode. The
138 quality of the assemblies was evaluated using QUAST (v5.2.0) (35), which provided metrics
139 such as number of contigs, length, and N50.

140 **Genome filtering**

141 For NIH data, contigs shorter than 500 base pairs or with coverage below 20x were removed.
142 For NCBI data, genomes with more than 300 contigs were excluded, and contigs shorter than
143 500 base pairs were removed. Potential sample contamination was assessed using CheckM
144 (v1.2.3) (36). Genomes with contamination levels exceeding 5% or completeness below 90%
145 were excluded from subsequent analyses.

146 **Core genome analysis**

147 Assembled genomes were annotated with Prokka (1.14.6) (37) with the annotation from
148 assembly ASM1672882v1 (strain FDAARGOS_1091) used as a reference database. Core
149 genome analysis was performed using the Panaroo pipeline version 1.5.0 (38) with a protein

150 sequence identity threshold of 90%, gene length coverage cutoff of 75%, and a core genome
151 sample threshold of 0.95.

152

153 **Phylogenetic analysis of *Achromobacter xylosoxidans***

154 Phylogenetic analysis of NIH and NCBI data was performed using kSNP4 (39). The optimal k-
155 mer size was determined using Kchooser. kSNP4 was run with the selected k-mer size, and a
156 parsimony tree was generated based on SNP loci present in at least 95% of the genomes. For
157 NIH data, in addition to kSNP4, RaxML (40) was used to construct the phylogenetic tree.
158 Briefly, core genes identified by Panaroo were used as input. RAxML v8.2.12 (40) was
159 utilized to build a rooted maximum likelihood tree using the general time-reversible (GTR)
160 substitution model with gamma correction to account for rate variation among sites. Since
161 the phylogenetic trees generated by kSNP4 and RAxML were identical, only one tree was
162 reported. The final tree was visualized using iTOL (41).

163

164 **Population structure analysis**

165 The genome-wide haplotype data were calculated as described previously (42). SNP calling
166 was performed for core genes identified by the panaroo pipeline, and imputation for
167 polymorphic sites with a missing frequency of less than <1% was conducted using BEAGLE
168 v.3.3.2 (43). This genome-wide haplotype dataset contained 144,290 SNPs, which was used
169 to define isolate populations and subpopulations based on haplotype profile similarity.
170 fineSTRUCTURE analysis (44) was performed with 200,000 iterations of both the burn-in and
171 Markov chain Monte Carlo (MCMC) method to cluster individuals based on the coancestry
172 matrix, as previously described (45). The results were visualized as a heat map, with each
173 cell representing the proportion of DNA a recipient receives from each donor.

174

175 **Variant calling**

176 The variants were called with Snippy v4.4.0 (https://github.com/tseemann/snippy), with
177 default option. NIH-016-2, collected first in the NIH-016 series, was used as a reference.

178 **Secretion system analysis**

179 Secretion systems and appendages were identified using MacSyFinder 2.1.3 (46). TXSScan
180 was run to search for all types of secretion systems and appendages, including T1SS, T2SS,
181 T3SS, T4SS, T5SS, T6SS, Flagellum, Tad pilus, and T9SS. CONJScan was run to detect
182 conjugative and mobilizable elements, which include T4SSs. The ”ordered replicon” option
183 was used for our complete genome sequences.

184 For genomes in which the secretion systems were not found by MacSyFinder, we manually
185 looked up for key genes of the systems in the annotated genomes, as it is possible that the
186 segmentation of the sequences that feed into MacSyFinder interferes with the gene search.
187 These are also key genes used by MacSyFinder. A system was noted as absent when none of
188 the genes were found.

189

190 **Phylogenetic analysis of T3SS**

191 Amino acid sequences of SctN or its homologs were extracted from Uniprot and NCBI.
192 Multiple sequence alignment of SctN sequences was performed using MAFFT (47) with
193 default parameters. A rooted maximum likelihood tree was constructed using RAxML v8.2.12
194 (40) with the general time-reversible (GTR) substitution model and gamma correction for
195 rate variation among sites. The phylogenetic tree was visualized using iTOL (41).

196

197 **Structural Modeling of YscN ATPase**

198 The amino acid sequence of the T3SS ATPase from *A. xylosoxidans* was obtained from NCBI
199 with sequence ID of WP_020925211.1. Structure of YscN was predicted using AlphaFold via
200 the website: https://alphafoldserver.com/. The predicted structure of *Pseudomonas*
201 *aeruginosa* PA14 was downloaded from https://alphafold.ebi.ac.uk/entry/A0A2U2Y0I4 with
202 accession number of AF-A0A0H2Z9F1-F1. Structural alignment of the two proteins was
203 performed using Pymol (The PyMOL Molecular Graphics System, Version 3.0 Schrödinger,
204 LLC).

205

206 **Biofilm**

207 Bacterial cultures were initiated in glass culture tubes by inoculating bacteria from LB agar
208 plates into 1 mL of LB broth at a starting OD600 of 0.1. The cultures were then incubated
209 statically at 37°C for 3 days. On the third day, media was removed by pipetting, and biofilms
210 were washed with water and dried overnight at 37°C. The following day, a 1% crystal violet
211 solution was used to stain biofilms for 5 minutes, followed by additional washes with water
212 and overnight drying at 37°C. Biofilms were solubilized with 100% DMSO, and absorbance
213 was measured at 595 nm using a BioTek plate reader.

214

215 **Infection of *Achromobacter* in cell lines**

216 J774a.1 cells were seeded at a density of $6x10^4$ cells in 100 µL DMEM media in a tissue culture-
217 treated black flat-clear bottomed 96-well plate. On the day of infection, cells were washed
218 with PBS and incubated for one hour with OPTI-MEM media containing 200 ng/mL propidium

219 iodide (PI) and 1.45µM Hoechst 33342. *Achromobacter* inoculum was then prepared by
220 resuspending bacteria in OPTI-MEM. Cells were infected with the bacteria at multiplicity of
221 infection of 7 and spun down at 750 rpm for 5 minutes to synchronize infection. The 96-well
222 plate was then inserted into a stage incubator supplied with CO_2 and maintained at 37°C in a
223 Nikon AXR confocal fluorescent microscope. Three images of cells were taken at arbitrary
224 locations within each well and observed every hour for up to five hours. Cytotoxicity was
225 measured by the ratio of PI^+ signal to $Hoechst^+$ signal (dead cells/total cells) expressed in
226 percentage using ImageJ v 1.54g. PI^+ and $Hoechst^+$ cells were processed using background
227 subtraction, followed by gamma adjustment and median filtering. Then, Otsu method was
228 applied for thresholding, and cell counts were obtained using the Analyze Particles function.

229 **Swimming motility in *Achromobacter* strains**

230 Bacteria were inoculated and grown overnight in 1mL LB broth from single colonies on LB agar
231 plates. Overnight growth was measured by OD600 and concentrated to an OD600 of 10 in
232 100µL. 2µL of the resulting suspension was injected via pipette into 0.25% agarose 2%
233 tryptone plates. Plates were incubated at 37°C for 4 hours and imaged with a Chemidoc^{tm}
234 Imaging System using the stain free blot procedure with 3 second exposure time. The resulting
235 images were exported to ImageJ. Images were converted to an 8-bit format and a
236 brightness/contrast correction step was performed. The zone of motility was then selected
237 using the circle tool and resulting area in Pixels was exported. Pixel count was converted to
238 mm^2 using the formula: mm^2 = (Pixels)/(5000 Pixels /((3.5mm/2)^2*3.14159)).

239

240 ## 3. Results

241

242 **Genomic diversity of *Achromobacter***

243 To examine the diversity among *A. xylosoxidans* isolates, we analyzed the whole-genome
244 sequencing data from 48 *Achromobacte*r spp. isolates (including 34 *A. xylosoxidans*, and other
245 *Achromobacter* species collected at the NIH clinical center in the previous study (51) referred
246 to as NIH isolates) and 197 *A. xylosoxidans* genomes from NCBI (referred to as NCBI isolates).
247 Although our focus was on *A. xylosoxidans*, we included other *Achromobacter* species from
248 our NIH isolates as references to assess their clustering relative to *A. xylosoxidans*. The 197
249 NCBI isolates were predominantly from the United States (n = 51), Germany (n = 39), Russia
250 (n = 19), China (n = 12), and Australia (n = 11) (Figure 1). In this dataset, *A. xylosoxidans* isolates
251 were primarily collected from respiratory sources (e.g. cystic fibrosis patients), followed by
252 environmental samples (Figure 1A). Among the NIH isolates, the majority of samples were
253 collected from respiratory sources, with bloodstream isolates being the second most common
254 (Figure 1B).

255 From the NIH isolate sequence, genome assembly was performed and contigs greater than
256 500 bps with coverage of 20 or more were retained. CheckM analysis identified 10 genomes
257 with contamination levels exceeding 5%, which were removed from further analysis (Table
258 S1). This resulted in 38 genomes from the NIH isolate dataset, including 24 *A. xylosoxidans*
259 isolates. For the NCBI genomes, those with more than 300 contigs were excluded, and contigs
260 shorter than 500 bps were removed, resulting in 141 genomes. One genome was further
261 excluded due to low genome completeness (less than 70%) (Table S1). This yielded a final
262 dataset of 178 genomes for downstream analysis.

263 We first examined the core genome of these isolates. Using the Panaroo pipeline, we
264 identified 3,387 core genes (present in at least 95% of the isolates), representing 53% of total
265 genes in *A. xylosoxidans* (Table 1). The remaining 47% of genes were classified as accessory
266 genes, highlighting the genomic plasticity of this species. Phylogenomic analysis of the core
267 genomes of all 178 isolates revealed significant diversity, with isolates largely being nonclonal
268 (Figure 2). NIH isolates were scattered among NCBI isolates, and clustering did not correlate
269 with geographical locations or sample sources. A group of environmental isolates formed a
270 distinct cluster (except for NIH-006-1), while others clustered with NIH clinical isolates,
271 underscoring the complexity of *A. xylosoxidans*. Non-*A. xylosoxidans* isolates clustered
272 together (except for one isolate NIH-021-1), suggesting the ability of this analysis to
273 differentiate *Achromobacter* species. In co-ancestry analysis, there are a few cases with some
274 level of shared ancestry from environmental samples. However, most isolates are unrelated
275 to each other, suggesting that they are genetically diverse and likely evolve independently
276 (Figure S1).

277 We also specifically looked at the phylogenetic analysis of the *A. xylosoxidans* genomes from
278 the NIH isolates (Figure 2B). In this data, isolates collected from the same patients over time
279 have the same middle number. For example, NIH-016-2 and NIH-016-3 were from the same
280 patients; or NIH-010-3, NIH-010-4, NIH-010-6 were from the same patients. Phylogenetic
281 analysis using two methods, kSNP or Panaroo followed by RaxML (see Methods section for
282 details) yielded identical phylogenetic trees for the NIH isolates data, suggesting the
283 robustness of the phylogenetic reconstruction. The analysis showed that isolates collected
284 from the same patients clustered together, indicating genetic similarity and suggesting
285 persistence and evolution within the same host over time. The only exception was NIH-005-4,
286 which did not cluster with NIH-005-2 and NIH-005-3. NIH-005-4 was collected from sputum in
287 2014, whereas NIH-005-2 and NIH-005-3 were collected from the perirectal region and
288 bronchoalveolar lavage, respectively, in 2016.

289

290

291 **Antibiotic resistance in *Achromobacter***

292 Antibiotic susceptibility data of NIH isolates revealed a prevalence of multidrug-resistant
293 *Achromobacter* spp. among the 12 antibiotic tested, including CZA (Ceftazidime/Avibactam),
294 C/T (Ceftolozane/Tazobactam), IMR (Imipenem/Relebactam), MERO (Meropenem), AZT/ATM
295 (Aztreonam), FEP (Cefepime), TAZ (Ceftazidime), CIP (Ciprofloxacin), IMI (Imipenem), LEVO
296 (Levofloxacin), PT4/TZP (Piperacillin/Tazobactam), and SXT (Trimethoprim/Sulfamethoxazole)
297 ((51), Figure 3A). Many AR genes were identified in the NIH isolates using the CARD
298 database; however, these genes could not fully explain the AR in certain isolates (51). Two
299 notable isolates, NIH-016-2 and NIH-016-3, were collected from the same patient. However,
300 NIH-016-3 was resistant to 11 antibiotics (all antibiotic tested except SXT), while NIH-016-2
301 was resistant to only three. Antimicrobial Resistance analysis using CZ ID website (52)
302 showed that NIH-016-2 and NIH-016-3 isolates carried similar sets of AR systems, including
303 efflux pumps (AdeFGH, AxyXY-OprZ, MexAB-OprM, MuxABC–OpmB, MexGHI-OpmD,
304 MexCD-OprJ, MexJK-OprM, MexPQ-OpmE), OXA-114h β-lactamase, AXC β-lactamase, and
305 CatB. Thus, we re-sequenced both NIH-016-2 and NIH-016-3, as well as NIH-016-1, which
306 has the same level of antibiotic resistance as NIH-016-3 and was collected after NIH-016-2.
307 Using both short reads and long read sequences, we were able to assemble complete
308 genomes of the three isolates. Then, variant analysis was done using NIH-016-2 as a
309 reference (Table 3). Interestingly, the variant analysis identified a T>G single nucleotide
310 polymorphism (SNP) at position 29 of AxyZ, resulting in a nonsynonymous mutation (V29G)
311 in both NIH-016-3 and NIH-016-1. AxyZ is a negative regulator of AxyXY-OprZ RND efflux
312 pump. This mutation is associated with overexpression of AxyXY-OprZ efflux pump, which
313 may involve in resistance against multiple antibiotics including tobramycin, gentamicin,
314 cefepime, ofloxacin, and levofloxacin (53). Thus, it is possible that the mutation is
315 contributing to higher resistance to resistance to FEP and LEVO in NIH-016-3 and NIH-016-1.

316

317 Several other SNPs that may involve in antibiotic resistance were found. A few of them have
318 been found to be involved in antibiotic resistance in other bacteria. A T>A SNP at position 695
319 of MutL in NIH-016-3 was identified. This mutation results in a nonsynonymous mutation from
320 leucine to glycine (Leu232Gly). MutL, along with MutS and UrvD belong to mismatch repair
321 system responsible for DNA repair. Mutations in MutL and MutS are associated with
322 hypermutator phenotype and higher antibiotic resistance in *P. aeruginosa* (54). Similarly, MutS
323 deletion has been associated with hypermutation and identified as an important adaptive
324 mechanism of *A. xylosoxidans* during chronic infection (55). Thus, this mutation might be
325 another potential contributor to higher resistance in NIH-016-03. A variant T>C at position
326 2228 in *mfd* gene which led to a change from leucine to proline (Leu743Pro) mutation was
327 identified. This gene has been associated with increasing rate of mutagenesis and the
328 development of antibiotic resistance (56). Additionally, C>T SNP leading to a change from
329 arginine to cysteine (Arg198Cys) mutation in ABC transporter substrate-binding protein was
330 identified. ABC transporters are essential in controlling the uptake and efflux of different
331 substrates including antibiotics in a bacterial cell (57). Overall, there are at least three SNPs
332 potentially impact AR of NIH-016s, that requires further study.
333 **Secretion systems in *Achromobacter xylosoxidans* clinical isolates**

334 Previous studies have shown that *A. xylosoxidans* can express multiple virulence factors,
335 including secretion systems and flagella (15, 23). We performed a bioinformatics analysis to
336 identify secretion systems and flagella in the 24 *A. xylosoxidans* NIH isolates. The reference
337 genome (FDAARGOS_1091) and two additional clinical isolates (GN050 and GN008) were
338 included for comparison (Table 3). All isolates possessed T1SS, T2SS, T5SS, and bacterial Tight
339 adherence Secretion System (TadSS). T6SS was present in all isolates except NIH-021-1, and
340 T4SS was present in all isolates except NIH-009-1. Interestingly, although a number of isolates
341 were collected from the same patients over time, most of them still carry flagella genes and
342 T3SS. Only one isolate, NIH-023-1 doesn't encode for either the flagellar system or the T3SS.

343

344 The type III secretion system is an important virulence mechanism contributing to cytotoxicity
345 in *A. xylosoxidans* (12, 15). Thus, we examined the T3SS in *A. xylosoxidans* more closely.
346 Phylogenetic analysis showed that the T3SS in *A. xylosoxidans* belongs to the Ysc T3SS family
347 (Figure 4A), which includes T3SS from other pathogens such as *P. aeruginosa*, *Yersinia*
348 *pseudotuberculosis,* and *Bordetella pertussis*. Structural modeling of the APTase YscN from *A.*
349 *xylosoxidans* showed high similarity to that of *P. aeruginosa* PA14, with a root-mean-square
350 deviation (RMSD) of 0.488 A^{o} (Figure 4B). This structural similarity further supports the
351 classification of *A. xylosoxidans* T3SS within the Ysc family.

352 **Cytotoxicity in *Achromobacter***

353 Previous studies have shown that T3SS expression correlates with cytotoxicity in infected host
354 cells (12, 15). To assess the cytotoxicity of the NIH isolates, we infected macrophage J774.a.1
355 with each isolate and measured cell death over time. We included two clinical isolates, GN050
356 and GN008, which were previously reported to exhibit differential cytotoxicity, as controls
357 (15). The result showed that the 24 isolates have variable cytotoxicity levels with NIH-018-1
358 being the most cytotoxic, exceeding that of GN050 (Figure 5). Among clinical isolates no
359 measurable difference was detected between the isolate source, and no clear pattern was
360 apparent in isolates collected at subsequent time points. Among the isolates collected from
361 the same patients, NIH-010 and NIH-016 had minal cytotoxicity, while NIH-025 are cytotoxic.
362 In NIH-018 series, the bacteria seemed to be more virulence over time. Most cytotoxic isolates
363 possess T3SS and AxoU (Table 3), with one exception. Isolate NIH-019-1 has an intermediate
364 cytotoxicity level, but it doesn't encode AxoU, although it has T3SS. This may suggest the
365 presence of (an) uncharacterized effector(s).

366 **Biofilm**

367 The capacity of a bacterium to form biofilms is a strong indicator of virulence and can be tied
368 to the expression of other virulence factors (58) (59) (60). Additionally, biofilm formation
369 improves the resistance of the organism to antibiotic and environmental pressures. We
370 therefore set out to examine biofilm formation in static culture of *A xylosoxidans*. *P.*
371 *aeruginosa* PA01 Δ*wspF*Δ*pelA*Δ*pslBCD* was used as negative control and PA01 Δ*wspF* as a

372 positive control (61, 62) for biofilm formation. GN050 showed robust biofilm formation
373 compared to the control (Figure 6). Most NIH isolates demonstrated a low level of biofilm
374 production. Only NIH-016-1, NIH-021-1 and NIH-025s displayed substantial biofilm forming
375 capabilities over the negative control. These isolates were from sputum (NIH-016-1), wound
376 (NIH-021-1), blood or lung (NIH-025s), suggesting that the source of isolation does not
377 determine whether the bacteria can form biofilm. The intra-host series, NIH-010, NIH-016 and
378 NIH-018 do show a trend of increasing biofilm production although it's not statistically
379 significant from the *P. aeruginosa* negative control.

380 ***Achromobacter* Flagellar Motility**

381 Flagellar motility is an important virulence factor which the bacteria employ to move to the
382 site of infection and is often coordinated with the expression of other virulence genes (63-65).
383 During prolonged infection, mutation in flagellar genes can accumulate resulting in an overall
384 loss of flagellar production (66). We decided to investigate the flagellar motility of our *A.*
385 *xylosoxidans* clinical isolates to determine if our strains demonstrate any changes in motility.
386 Our results demonstrated substantial differences in flagellar motility between strains even
387 from isolates collected from the same patients (Figure 7A). The most motile isolates are NIH-
388 003-1, NIH-005-4, NIH-014-1, NIH-016-2, NIH-018-3, and NIH-026-1. Samples isolated from
389 respiratory systems showed a greater tendency to lose motility compared to those from skin
390 or wound infections (Table 3). Among all 14 respiratory isolates (NIH-005-3, NIH005-4,
391 NIH009-1, NIH010-3, NIH-010-4, NIH-014-1, NIH016-2, NIH016-3, NIH018-1, NIH018-2,
392 NIH019-1, NIH022-1, NIH023-1, and NIH025-6) 8 were identified as non-motile representing
393 57.1% of the group. Additionally, among all non-motile isolates, 80% were isolated from a
394 respiratory source. Comparing strains isolated at different times from the same patient, NIH-
395 005, NIH-010, and NIH-016 series showed a loss of motility whereas NIH-018 series showed
396 reduced motility. In NIH-005 series, isolate 2 and 3 were collected in the same year, two years
397 after isolate 4. The isolates 2 and 3 don't move while isolate 4 demonstrates high motility
398 among all isolates. This also supports the phylogeny finding that isolate 4 is different from
399 isolates 2 and 3. In isolates NIH-010 series, isolate 6 was more motile than isolates 3 and 4,
400 which were isolated after isolate 6. In series NIH-018, NIH-018-3 is one of the best swimmers.
401 The motility reduced about 50% after one and two years in the subsequent isolates, but they
402 are still motile. These observations indicate a preference for a reduction of flagellar function
403 in the respiratory environment.

404 The NIH-016 series demonstrated some of the most substantial differences in motility
405 between isolates. We investigated the genomic differences present among genomes of NIH-
406 016 series. Multiple sequence alignment between known flagellar genes in NIH-016-2
407 compared to the genome of NIH-016-3 showed near perfect identity between the isolates
408 except for two identified point mutations in *fliO* and *flhF* (supplemental table 1). The point
409 mutation in *fliO* when translated results in a synonymous mutation. However, a T>G single
410 nucleotide polymorphism was identified in *flhF* which resulted in a Y330H mutation FlhF

411 (Figure 7B). This mutation also exists in NIH-016-1 which was collected after NIH-016-3. FlhF
412 is a GTPase known to be important for the initial insertion of flagellar components in the
413 membrane of the bacteria. Deletion or mutations of key regions of this protein are known to
414 result in non-flagellated bacteria and thus a loss of motility (67, 68).

415 Characterization of the protein for domains by InterProScan (69) revealed a predicted SRP54-
416 type protein, GTPase domain which spans from 329 to 520. SRP54-type proteins represent
417 signal recognition particles which bind GTP and are important for trafficking to the plasma
418 membrane (68, 70). This observation is in line with the predicted function of FlhF as a GTP
419 binding protein and its function in nucleating flagellar assembly in other bacteria (71, 72).
420 Prediction of the FlhF protein overall via modeling in alphafold (73) revealed four distinct
421 structures. A structure ranging from 268 to 520 comprised a GTPase domain. Alphafold
422 modeling of NIH-016-2 FlhF and NIH-016-3 FlhF and subsequent alignment revealed a
423 structural abnormality in NIH16-3's FlhF which resulted in a predicted displacement of a valine
424 at position 329 (Figure 7C). FlhF is known to homodimerize following binding to GTP (70) and
425 therefore we generated an additional model to visualize plausible homodimer structures of
426 NIH-0016-2 FlhF. Y330 was observed on the outside of the predicted model, indicating that
427 the mutation may not be causing any structural disruptions directly responsible for
428 dimerization (Figure 7D). An alternative hypothesis is the mutation may be disrupting the GTP
429 binding domain. An alignment of the predicted *Achromobacter* FlhF structure to the known
430 crystal structure of FlhF in *B. subtilis* showed a R^2 of 2.082, demonstrating they are structurally
431 similar. The known location of the GTP binding domain of *B. subtilis* FlhF is in close proximity
432 to the β-sheet containing the Y330H mutation (7E). Using observed differences in flagellar
433 motility we were able to identify a mutation in NIH-016-3 and NIH-016-1 which may be
434 contributing to a loss of flagellar motility possibly by the disruption of GTP binding. Overall,
435 these results demonstrate the varying dynamics of flagellar motility of *Ax* clinical isolates and
436 a loss of flagella activity during chronic infection.

437

438

439

440

441

442

443

4. Figures and tables

Figure 1: Geographic locations and collection source of samples used in this study. (A) The number of isolates collected in different countries around the world. (B) The number of isolates collected from different sources.

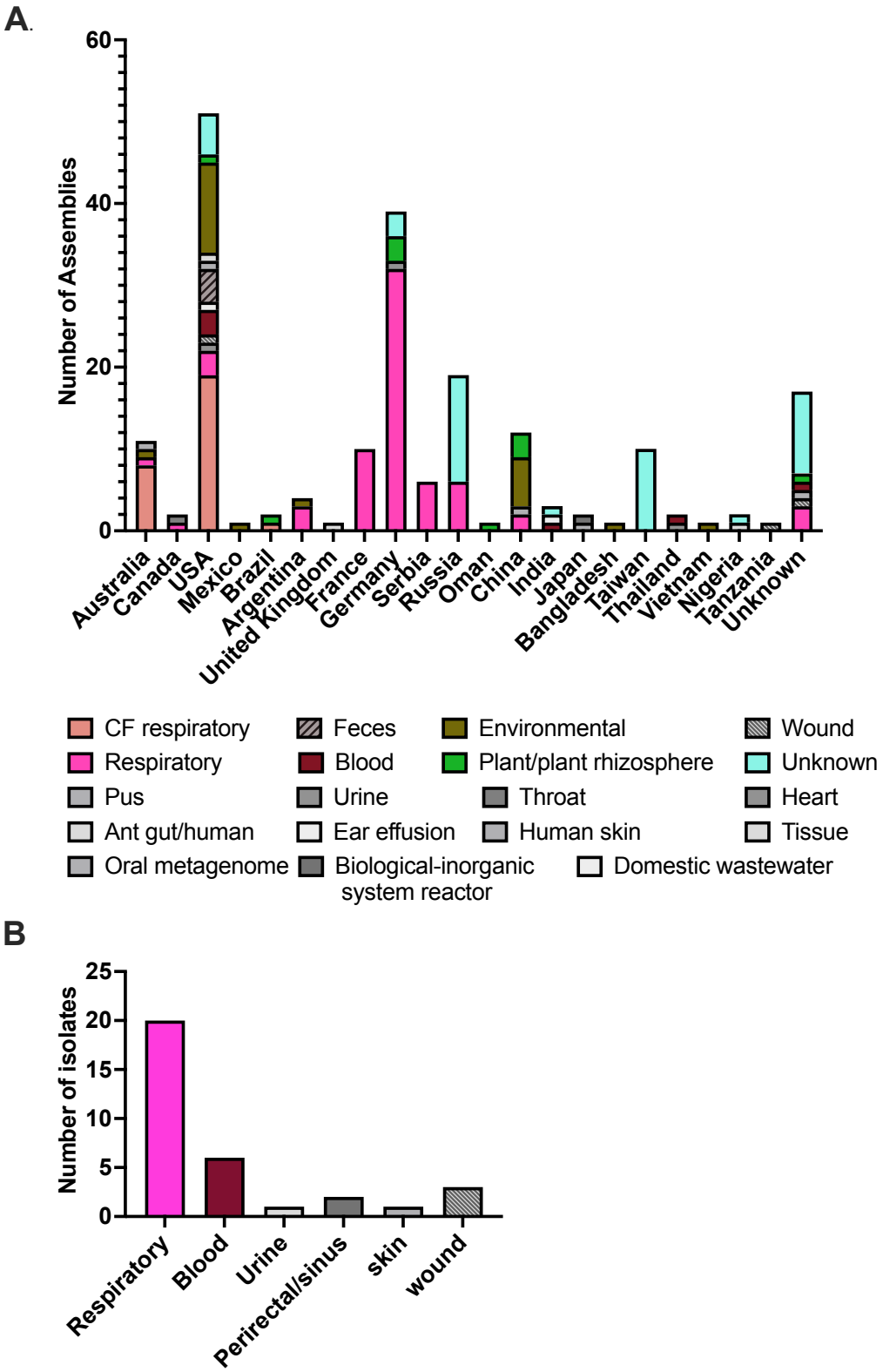

Figure 2: Phylogenetic tree of *Achromobacter.* A. Phylogenetic tree of all isolates. Environmental isolate cluster was labeled in green color. Clusters that contained mostly non *A. xylosoxidans* were labeled in blue. **B**. Phylogenetic tree of NIH *A. xylosoxidans* isolates.

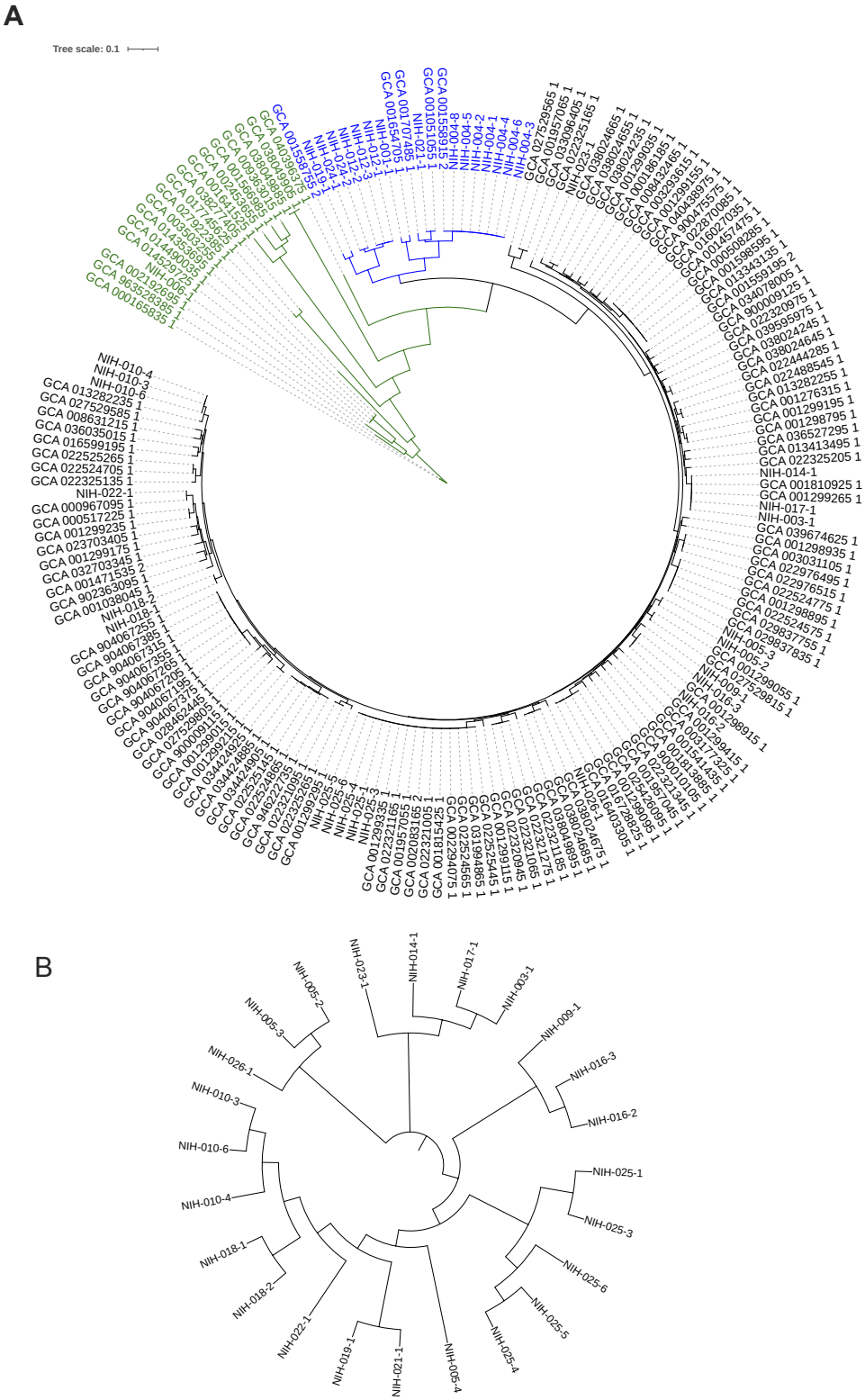

454 **Figure 3: Frequency of antibiotic resistance in NIH isolates.** (A) Antibiotic resistance in
455 NIH clinical isolates. The number of antibiotics out of 11 tested that each isolate was
456 resistant to was plotted. (B) Percentage of isolates resistance to each antibiotic was shown.

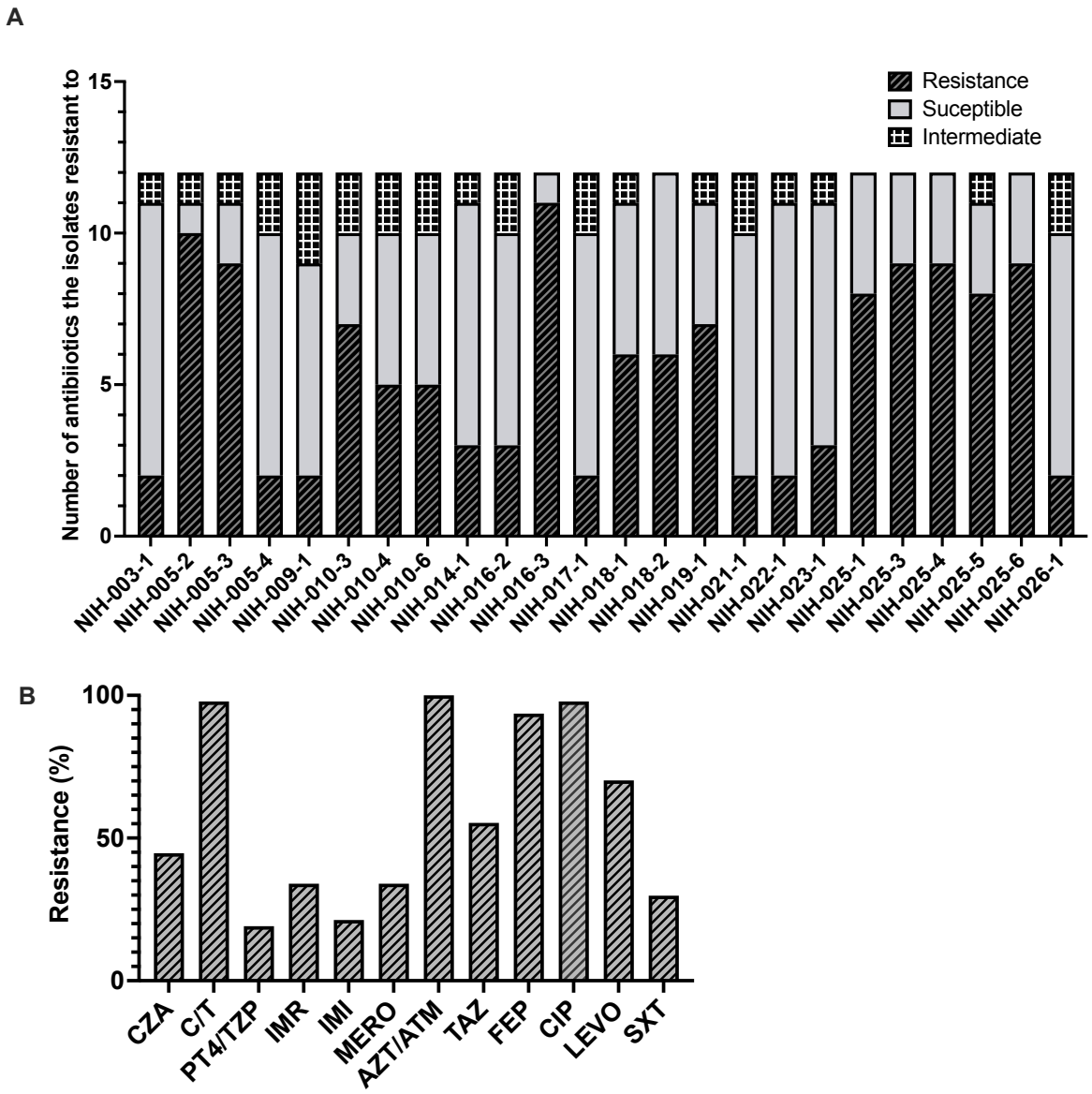

457

458

459

460

461

462

463

464

465 **Figure 4: The type III secretion phylogeny and structure.** A. Phylogenetic tree of T3SS families.
466 The tree was prepared using aligned amino acid sequence of SctN and its homologs. **B**
467 Predicted structure of YscN from *A. xylosoxidans*. **C.** Predicted structures of *A. xylosoxidans*
468 YscN (Orange color)and *Pseudomonas aeruginosa* PA14 PscN (blue color) superimposed.

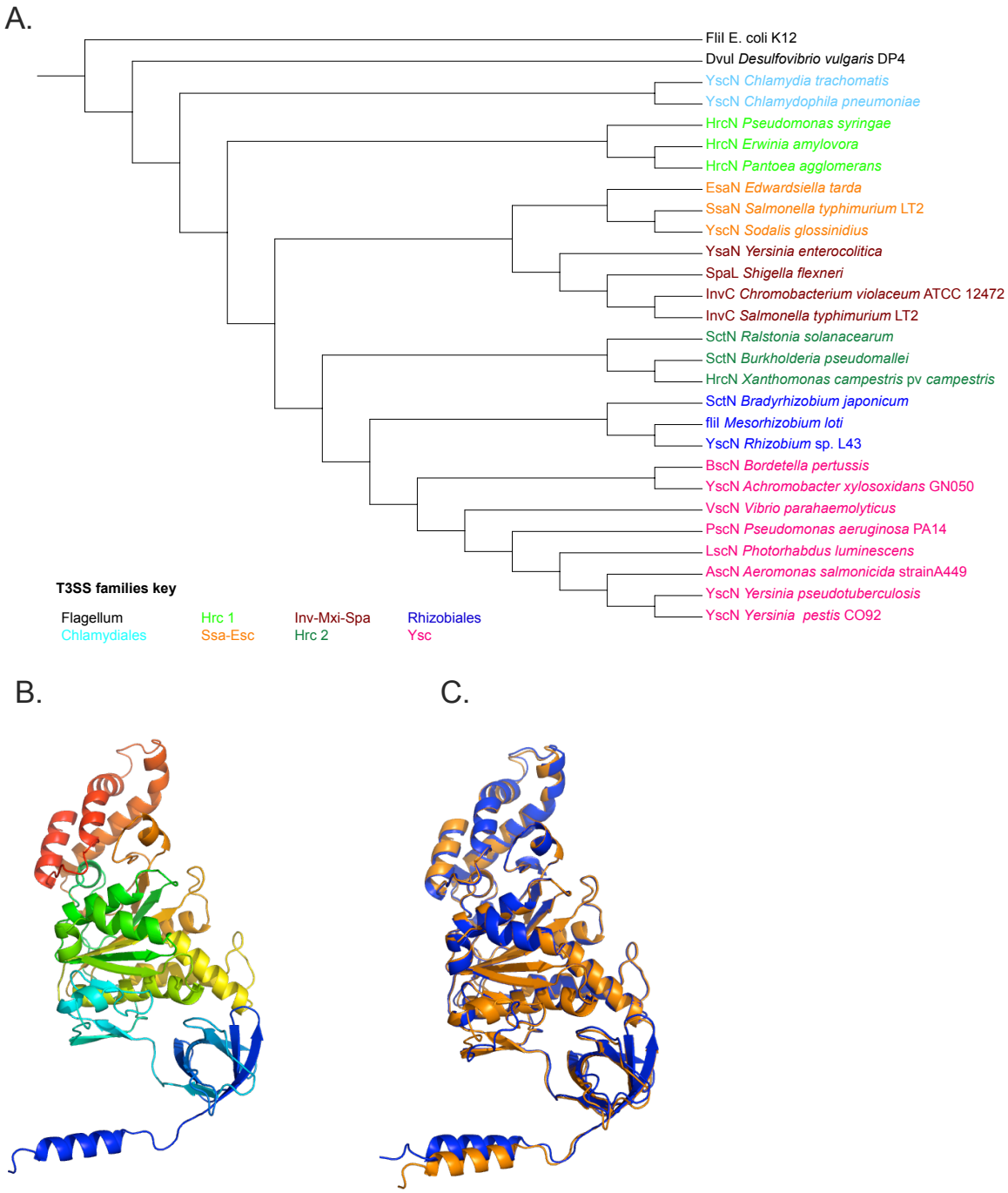

469

470

471

472

473

Figure 5: Cytotoxicity of *A. xylosoxidans* clinical isolates. (A) Cell death of macrophage J774a.1 cells infected with selected clinical isolates of *A. xylosoxidans* over time. (B) Cell death of macrophage J774a.1 cells infected with different clinical isolates of *A. xylosoxidans* at 5hai. Percent cell death - the ratio between dead cells and total cells - were shown. Different colored dots are for different biological replicates. Each isolate was experimented for at least two biological replicates, three technical replicate each time.

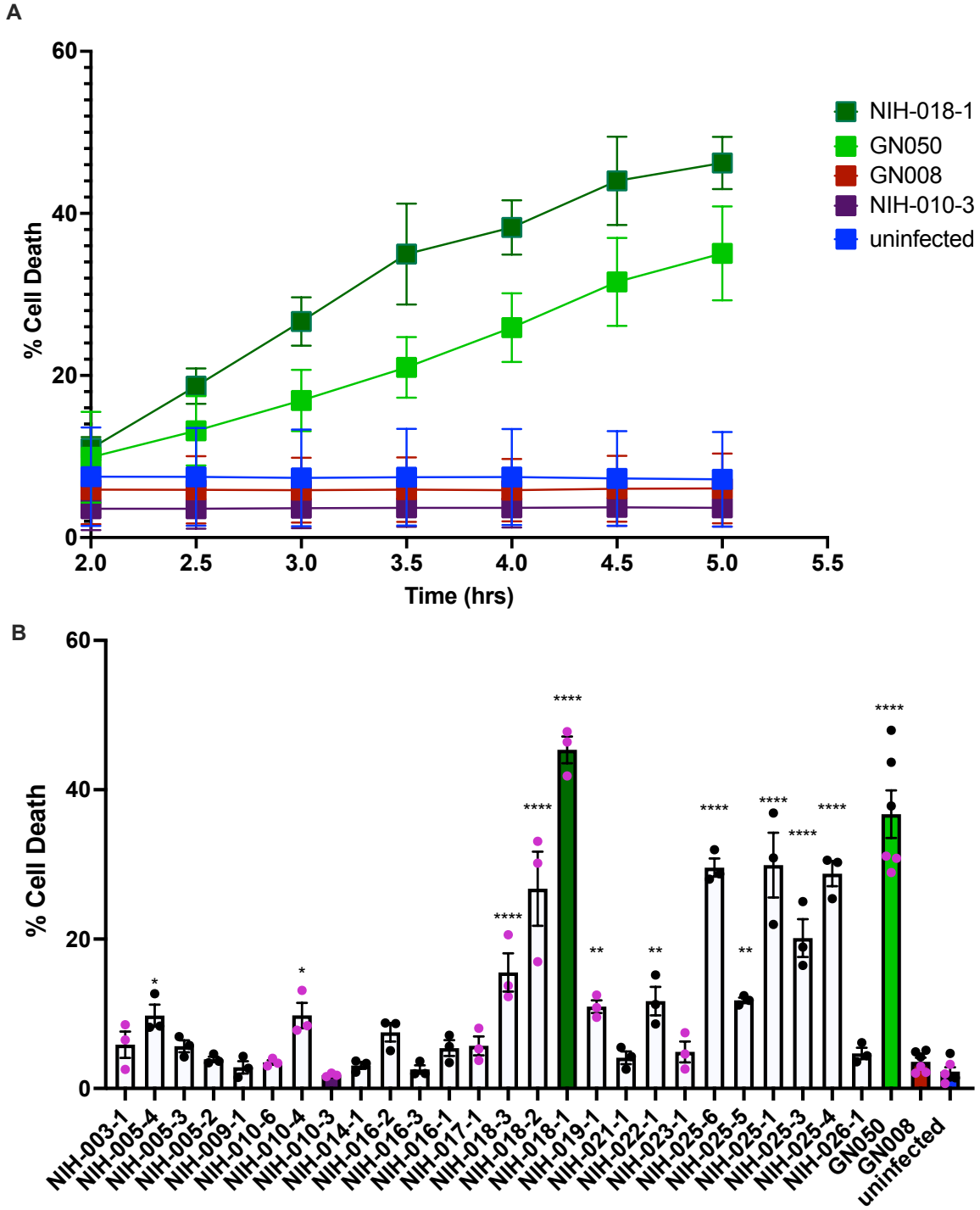

Figure 6: Biofilm formation by *A. xylosoxidans* clinical isolates. PA01 Δ*wspF*Δ*pelA*Δ*pslBCD* was used as a negative control. PA01 Δ*wspF* was used as a positive control. Different color dots indicate different biological replicates. The experiment was done in at least three technical replicates. Kruskal-Wallis test was done followed by Dunn's multiple comparisons to correct for multiple comparison. **** P-val <0.0001, *** P-val <0.0002, ** P-val <0.002, *P-val <0.0332.

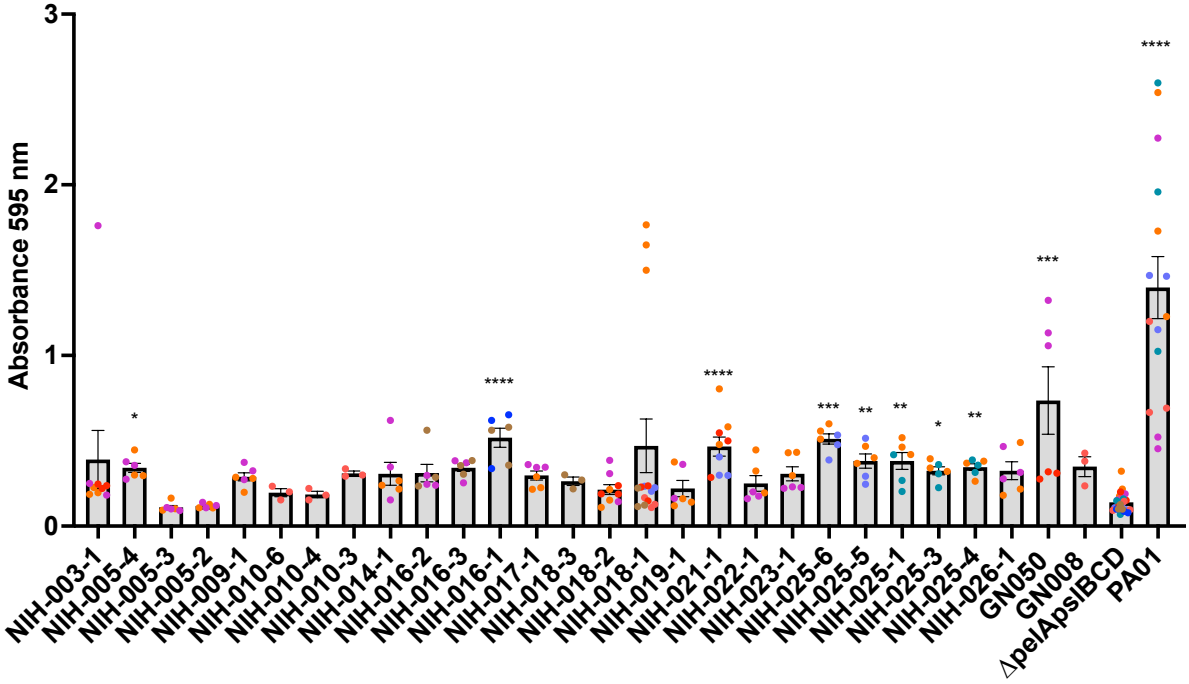

Figure 7: *A. xylosoxidans* motility. (A) *A. xylosoxidans* demonstrates substantial differences in flagellar motility among clinical isolates. (B) NIH-016-3 FlhF contains a point mutation resulting in a Y330H. (C) Mutation Y330H results in a predicted displacement of V229 (Purple) as determined by modeling in Alphafold (Blue: NIH-016-2 FlhF, Red: NIH-016-3 FlhF). (D) Alignment of monomeric NIH-016-2 FlhF (Blue) to homodimerized NIH-016-2 FlhF (Yellow). (E) Alignment of NIH-016-2 (Blue) to *B. subtilis* FlhF (Green) with bound GTP (Red).

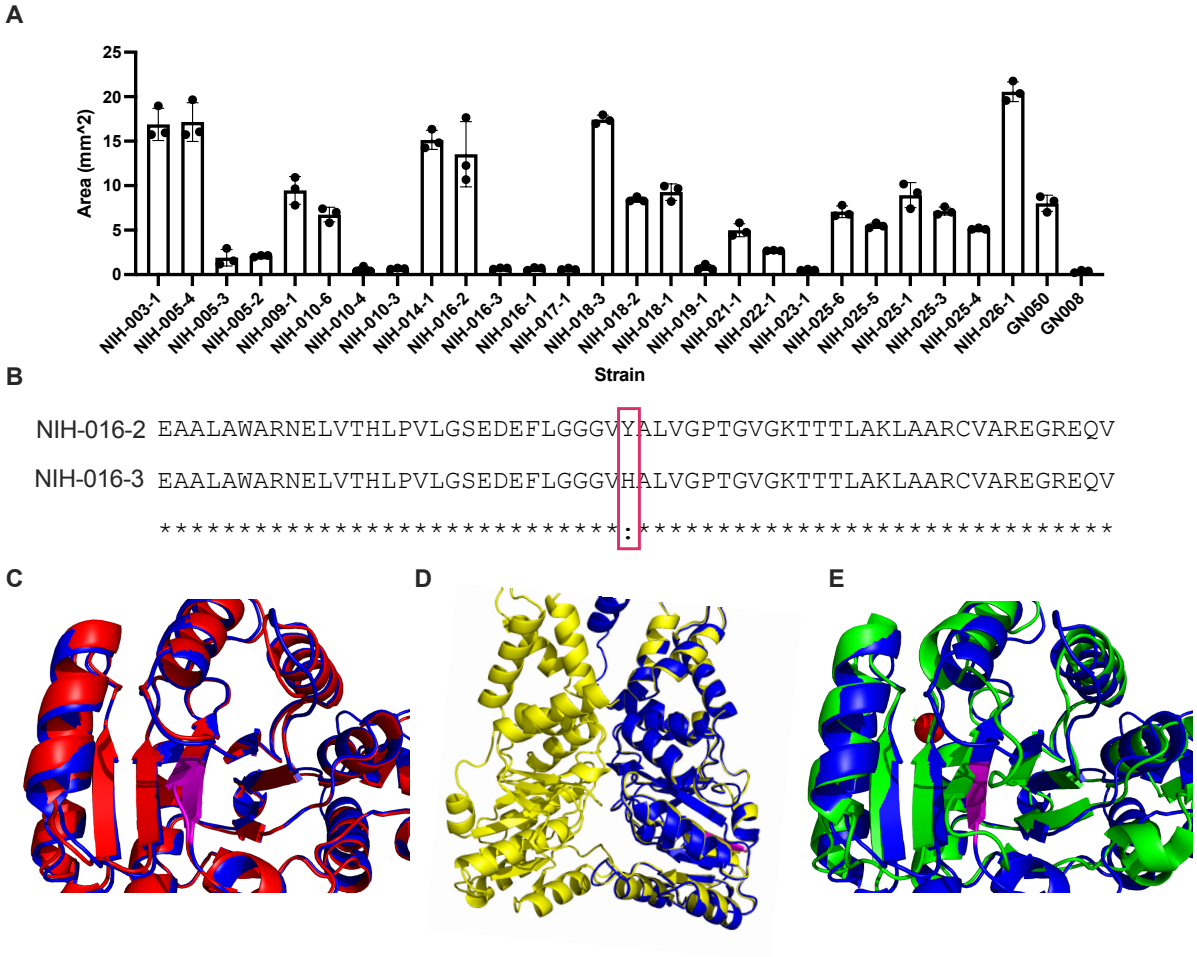

Figure S1: Co-ancestry analysis based on fineSTRUCTURE. The color of each cell in the matrix indicates the expected number of chunks imported from a donor genome (column) into a recipient genome (row). The sample source (A) and top six locations (B) were color coded next to the sample ID.

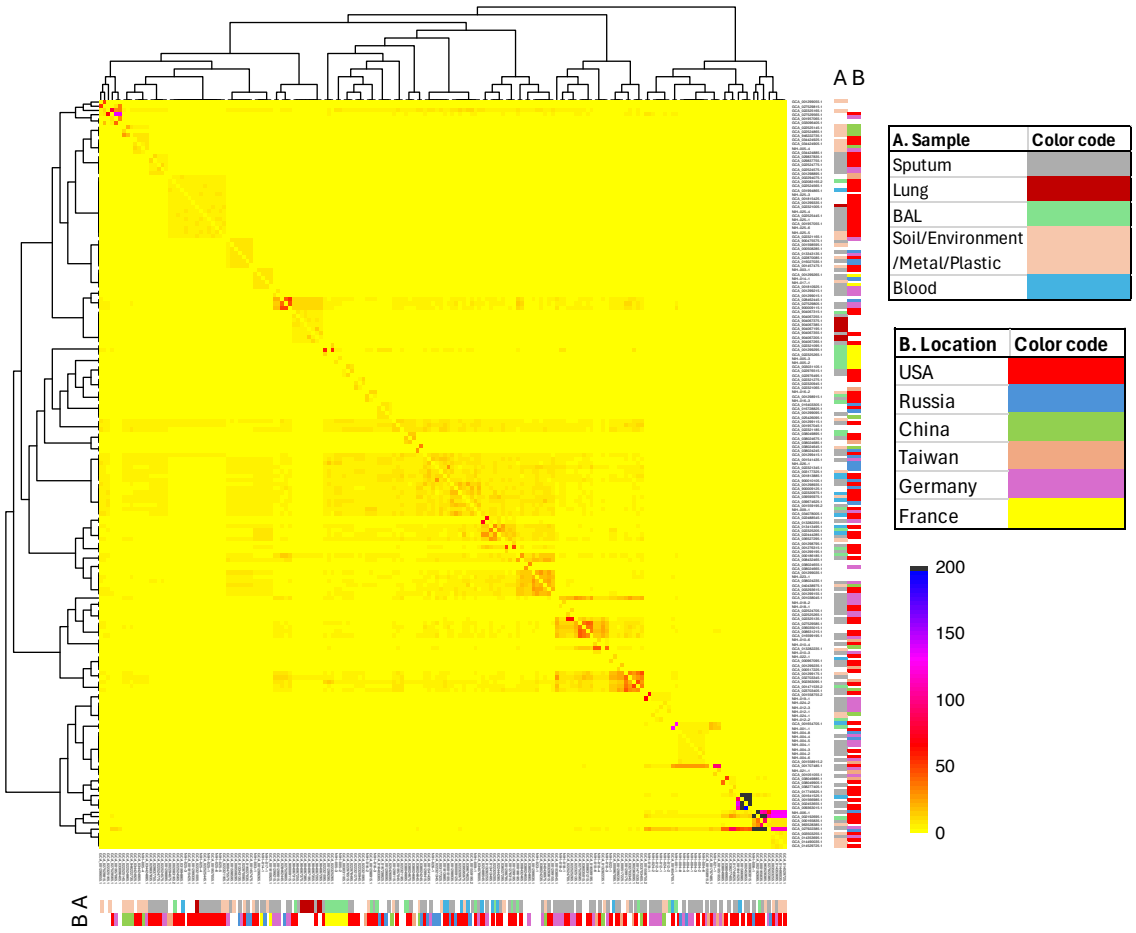

510 **Figure S2: Correlation of cytotoxicity, biofilm and motility.** Correlation between cytotoxicity
511 and motility (A), cytotoxicity and biofilm (B) and motility and biofilm (C), and biofilm and
512 antibiotic resistance (the number of antibiotic each isolate resistant to)

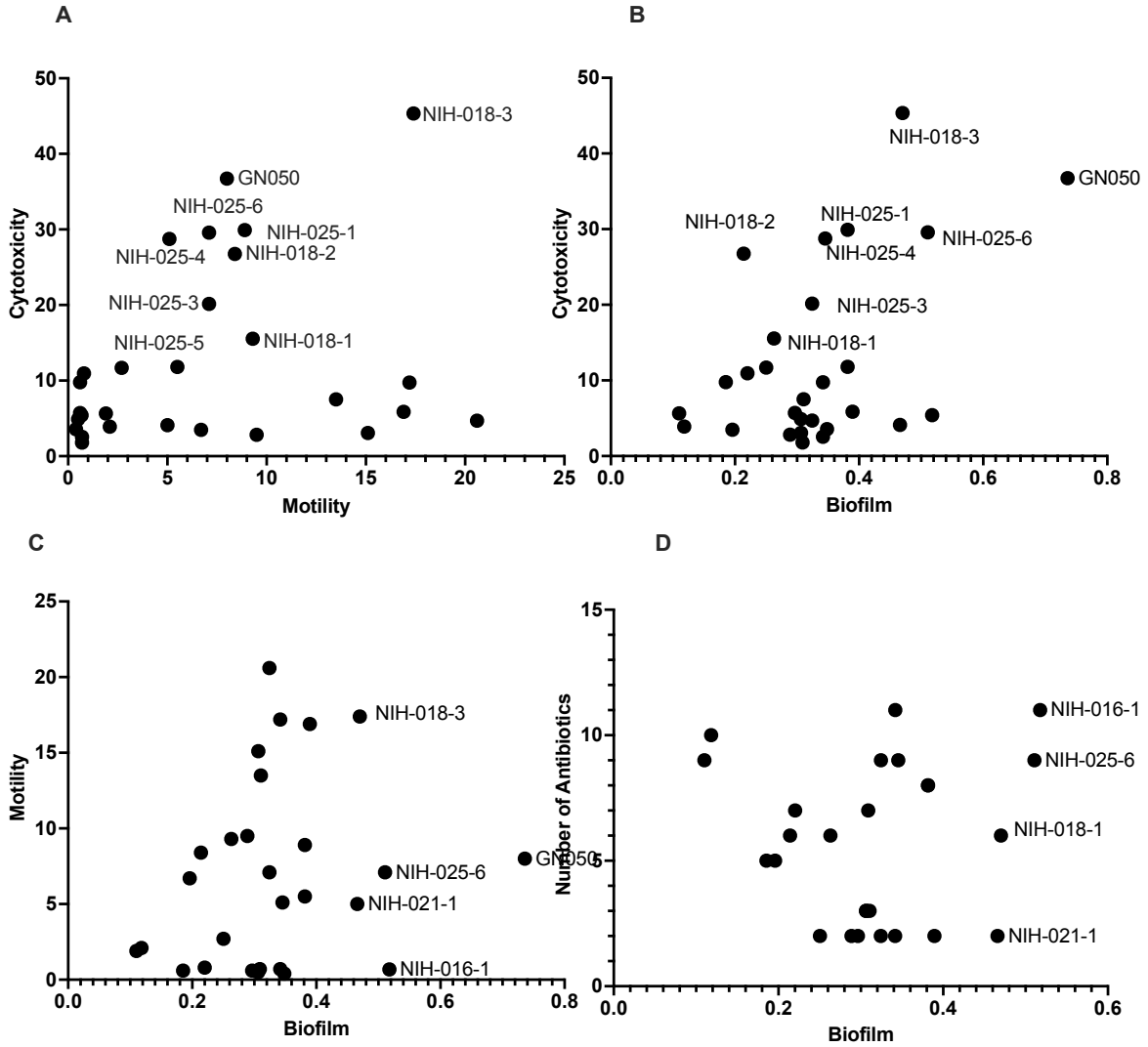

513
514
515

516

Table 1: Core genes in *Achromobacter xylosoxidans*

* Rare genes that occurs in less than 15% of isolates re not counted in the total genes to avoid underestimate the core gene for each genome.

Table 1A. core genes from 178 NIH and NCBI genomes	counts
Core genes (99% <= strains <= 100%)	2074
Soft core genes (95% <= strains < 99%)	1313
Shell genes (15% <= strains < 95%)	3066
Cloud genes (0% <= strains < 15%)	23298
Total genes *(15% <= strains <= 100%)	6453

Table 1B. core genes from 24 NCBI genomes	counts
Core genes (99% <= strains <= 100%)	4149
Soft core genes (95% <= strains < 99%)	588
Shell genes (15% <= strains < 95%)	2420
Cloud genes (0% <= strains < 15%)	3020
Total genes* (15% <= strains <= 100%)	10177

517

518

519 **Table 2: Summary of secretion system, motility, cytotoxicity, and biofilm of *A. xylosoxidans***
520 **isolates.** Three intra-host isolate series were highlighted in different colors. NIH-016-1 and
521 NIH-018-3 were included in the table for the analysis of intra-host samples, while the
522 genome sequencing were omitted in the phylogenetic analysis due to contamination issue.
523 [*]motility in mm^2
524 [#]cytotoxicity: percent cell death
525 [$] biofilm: Absorbance 595nm of crystal violet stained biofilm
526 [##] BAL: Bronchoalveolar lavage, AXL: Autopsy of the lung

Isoates	T1SS	T2SS	T3SS	T4SS	T5SS	T6SS	Tad	flagella	motility[*]	cytotoxicity[#]	presence of AxoU	Biofilm[$]	Total antibiotic resistance	collection date	Source[##]
NIH-003-1	yes	yes	yes	yes	yes	yes	yes	yes	16.9	5.9	yes	0.39	2	12/17/17	Wound
NIH-005-4	yes	yes	yes	yes	yes	yes	yes	yes	17.2	9.7	yes	0.34	2	10/10/14	Sputum
NIH-005-3	yes	yes	yes	yes	yes	yes	yes	yes	1.9	5.6	yes	0.11	9	10/30/16	BAL
NIH-005-2	yes	yes	yes	yes	yes	yes	yes	yes	2.1	3.9	yes	0.12	10	11/10/16	Perirectal
NIH-009-1	yes	yes	yes	no	yes	yes	yes	yes	9.5	2.8	yes	0.29	2	8/29/16	BAL
NIH-010-6	yes	yes	yes	yes	yes	yes	yes	yes	6.7	3.5	yes	0.20	5	9/4/12	Skin lesion
NIH-010-4	yes	yes	yes	yes	yes	yes	yes	yes	0.6	9.8	yes	0.19	5	7/26/13	BAL
NIH-010-3	yes	yes	yes	yes	yes	yes	yes	yes	0.7	1.8	yes	0.31	7	7/5/14	Sputum
NIH-014-1	yes	yes	yes	yes	yes	yes	yes	yes	15.1	3.1	yes	0.31	3	11/16/15	Autopsy lung
NIH-016-2	yes	yes	yes	yes	yes	yes	yes	yes	13.5	7.5	yes	0.31	3	7/15/14	Sputum
NIH-016-3	yes	yes	yes	yes	yes	yes	yes	yes	0.7	2.5	yes	0.34	11	2/11/15	Sputum
NIH-016-1	yes	yes	yes	yes	yes	yes	yes	yes	0.6805	5.4	yes	0.52	11	2/24/16	Sputum
NIH-017-1	yes	yes	yes	yes	yes	yes	yes	yes	0.6	5.7	yes	0.30	2	1/8/15	Nephrostomy urine
NIH-018-3	yes	yes	yes	yes	yes	yes	yes	yes	17.4	15.5	Yes	0.26	6	12/13/12	BAL
NIH-018-2	yes	yes	yes	yes	yes	yes	yes	yes	8.4	26.8	yes	0.21	6	11/8/13	Sputum
NIH-018-1	yes	yes	yes	yes	yes	yes	yes	yes	9.3	45.3	yes	0.47	6	1/22/14	Sputum
NIH-019-1	yes	yes	yes	yes	yes	yes	yes	yes	0.8	11.0	no	0.22	7	4/2/14	Sinus
NIH-021-1	yes	yes	yes	yes	yes	no	yes	yes	5.0	4.1	no	0.47	2	10/22/12	wound

NIH-022-1	yes	yes	yes	yes	yes	yes	yes	yes	2.7	11.7	yes	0.25	2	12/7/12	Sputum
NIH-023-1	yes	yes	no	yes	yes	yes	yes	no	0.5	4.9	no	0.31	3	3/22/13	BAL
NIH-025-1	yes	yes	yes	yes	yes	yes	yes	yes	8.9	29.9	yes	0.38	8	11/12/13	Blood
NIH-025-3	yes	yes	yes	yes	yes	yes	yes	yes	7.1	20.1	yes	0.32	9	11/20/13	Blood
NIH-025-4	yes	yes	yes	yes	yes	yes	yes	yes	5.1	28.8	yes	0.35	9	11/22/13	axl
NIH-025-5	yes	yes	yes	yes	yes	yes	yes	yes	5.5	11.8	yes	0.38	8	11/10/13	Blood
NIH-025-6	yes	yes	yes	yes	yes	yes	yes	yes	7.1	29.6	yes	0.51	9	11/9/13	BAL
NIH-026-1	yes	yes	yes	yes	yes	yes	yes	yes	20.6	4.7	yes	0.32	2	5/1/16	Wound (l heel)
GCA_016728825.1 (reference)	yes	yes	yes	yes	yes	yes	yes	yes	ND	ND	yes	ND	ND	4/30/18	Soil
GCA_013282235.1 (GN050)	yes	yes	yes	yes	yes	yes	yes	yes	8.0	36.7	yes	0.74	ND	7/12/10	Ear effusion
GCA_013282255.1 (GN008)	yes	yes	yes	yes	yes	yes	yes	yes	0.4	3.6	yes	0.35	ND	6/29/10	Cystic fibrosis sputum

527

Table 3: Changes of the genome between NIH-016-2 and NIH-016-1, NIH-016-3. NIH-016-2 was used as a reference. The mutations listed are the common mutations between NIH-016-3 and NIH-016-1, compared to NIH-016-2.

CHROM	POS	REF	ALT	EFFECT	LOCUS_TAG	PRODUCT
CP188777	5147082	G	GC	frameshift_variant c.1181dupC p.Pro395fs	ACP6EQ_23745	DUF3772 domain-containing protein
CP188777	5749106	G	GC	frameshift_variant c.1721dupG p.Ala575fs	ACP6EQ_26625	autotransporter domain-containing protein
CP188777	6041085	G	GC	frameshift_variant c.25dupC p.Leu9fs	ACP6EQ_27890	response regulator
CP188777	2069911	A	AC	frameshift_variant c.278dupC p.His94fs	ACP6EQ_09695	glycolate oxidase subunit GlcE
CP188777	6486625	CG	C	frameshift_variant c.421delG p.Glu141fs	ACP6EQ_29965	HIT family protein
CP188777	6419572	A	ACG	frameshift_variant c.481_482dupGC p.Tyr162fs	ACP6EQ_29660	dTDP-4-amino-4,6-dideoxygalactose transaminase
CP188777	4951892	G	GC	frameshift_variant c.73dupG p.Ala25fs	ACP6EQ_22700	PBSX family phage terminase large subunit
CP188777	4560728	G	GC	frameshift_variant c.839dupG p.Val281fs	ACP6EQ_20870	molybdopterin cofactor-binding domain-containing protein
CP188777	3770678	A	G	missense_variant c.1001T>C p.Val334Ala	ACP6EQ_17480	D-cysteine desulfhydrase family protein
CP188777	6213780	T	C	missense_variant c.1043T>C p.Val348Ala	ACP6EQ_28685	30S ribosomal protein S12

						methylthiotransferase RimO
CP188777	6348240	C	T	missense_variant c.104G>A p.Gly35Asp	ACP6EQ_29305	alpha/beta fold hydrolase
CP188777	306544	C	T	missense_variant c.106C>T p.Arg36Cys	ACP6EQ_01455	ornithine cyclodeaminase
CP188777	5614531	A	G	missense_variant c.10T>C p.Cys4Arg	ACP6EQ_26035	Bug family tripartite tricarboxylate transporter substrate binding protein
CP188777	6585839	C	T	missense_variant c.1195G>A p.Glu399Lys	ACP6EQ_30490	catalase
CP188777	2676682	C	T	missense_variant c.1264G>A p.Val422Met	ACP6EQ_12500	heavy metal translocating P-type ATPase
CP188777	785311	A	G	missense_variant c.1313T>C p.Leu438Pro	ACP6EQ_03715	ribonuclease catalytic domain-containing protein
CP188777	2395874	A	G	missense_variant c.133A>G p.Thr45Ala	ACP6EQ_11165	DUF5339 family protein
CP188777	5525409	T	C	missense_variant c.1396A>G p.Thr466Ala	ACP6EQ_25620	TonB-dependent siderophore receptor
CP188777	2107651	C	T	missense_variant c.146C>T p.Ser49Leu	ACP6EQ_09910	aromatic amino acid DMT transporter YddG
CP188777	5968107	A	G	missense_variant c.179A>G p.Asn60Ser	ACP6EQ_27535	prolyl aminopeptidase

CP188777	4914304	T	C	missense_variant c.1876A>G p.Thr626Ala	ACP6EQ_22475	TonB-dependent receptor
CP188777	1620551	A	G	missense_variant c.2228T>C p.Leu743Pro	ACP6EQ_07680	transcription-repair coupling factor
CP188777	4918789	T	C	missense_variant c.230T>C p.Val77Ala	ACP6EQ_22490	response regulator transcription factor
CP188777	3110891	T	C	missense_variant c.278A>G p.Tyr93Cys	ACP6EQ_14500	Bug family tripartite tricarboxylate transporter substrate binding protein
CP188777	2194430	A	G	missense_variant c.299T>C p.Val100Ala	ACP6EQ_10305	DUF3053 domain-containing protein
CP188777	1117935	C	T	missense_variant c.32G>A p.Gly11Asp	ACP6EQ_05315	polynucleotide adenylyltransferase PcnB
CP188777	5368021	A	G	missense_variant c.358A>G p.Thr120Ala	ACP6EQ_24820	protein translocase subunit SecD
CP188777	3172298	A	G	missense_variant c.415T>C p.Cys139Arg	ACP6EQ_14805	GMC family oxidoreductase
CP188777	36790	A	G	missense_variant c.41A>G p.Asp14Gly	ACP6EQ_00165	AraC family transcriptional regulator
CP188777	3111709	A	G	missense_variant c.422A>G p.Tyr141Cys	ACP6EQ_14505	LysR family transcriptional regulator
CP188777	5994882	T	C	missense_variant c.439A>G p.Ser147Gly	ACP6EQ_27665	RNA polymerase sigma factor

CP188777	896554	T	C	missense_variant c.443T>C p.Val148Ala	ACP6EQ_04250	MFS transporter
CP188777	2516449	C	T	missense_variant c.451C>T p.Arg151Cys	ACP6EQ_11765	class I SAM-dependent DNA methyltransferase
CP188777	3793425	AG	GC	missense_variant c.46_47delCTinsGC p.Leu16Ala	ACP6EQ_17565	cystathionine gamma-synthase family protein
CP188777	5023271	T	C	missense_variant c.464A>G p.Tyr155Cys	ACP6EQ_23155	4-hydroxythreonine-4-phosphate dehydrogenase PdxA
CP188777	444497	A	G	missense_variant c.472A>G p.Ser158Gly	ACP6EQ_02080	Bug family tripartite tricarboxylate transporter substrate binding protein
CP188777	1828128	A	G	missense_variant c.4874A>G p.Tyr1625Cys	ACP6EQ_08585	hemagglutinin repeat-containing protein
CP188777	1381223	A	G	missense_variant c.511A>G p.Thr171Ala	ACP6EQ_06610	glycosyltransferase family 9 protein
CP188777	2494682	G	A	missense_variant c.553G>A p.Gly185Ser	ACP6EQ_11675	copper-containing nitrite reductase
CP188777	3444638	G	A	missense_variant c.592C>T p.Arg198Cys	ACP6EQ_16040	ABC transporter substrate-binding protein
CP188777	6398223	T	C	missense_variant c.688T>C p.Tyr230His	ACP6EQ_29565	N-acetyl sugar amidotransferase

CP188777	1123581	A	T	missense_variant c.695T>A p.Leu232Gln	ACP6EQ_05345	DNA mismatch repair endonuclease MutL
CP188777	1351955	T	G	missense_variant c.700A>C p.Thr234Pro	ACP6EQ_06450	tyrosine-type recombinase/integrase
CP188777	755449	C	G	missense_variant c.700G>C p.Gly234Arg	ACP6EQ_03575	DUF342 domain-containing protein
CP188777	642598	C	T	missense_variant c.733G>A p.Glu245Lys	ACP6EQ_03095	bifunctional hydroxymethylpyrimidine kinase/phosphomethylpyrimidine kinase
CP188777	497968	A	G	missense_variant c.74T>C p.Val25Ala	ACP6EQ_02315	c-type cytochrome
CP188777	5144580	A	G	missense_variant c.74T>C p.Val25Ala	ACP6EQ_23735	acetyl-CoA hydrolase/transferase family protein
CP188777	5074135	A	G	missense_variant c.818T>C p.Val273Ala	ACP6EQ_23405	ABC transporter substrate-binding protein
CP188777	1704773	C	T	missense_variant c.848G>A p.Arg283His	ACP6EQ_08075	Bug family tripartite tricarboxylate transporter substrate binding protein
CP188777	1587091	T	G	missense_variant c.86T>G p.Val29Gly	ACP6EQ_07535	multidrug efflux transcriptional repressor AxyZ
CP188777	2510615	G	C	missense_variant c.88G>C p.Val30Leu	ACP6EQ_11745	SDR family oxidoreductase

CP188777	1924181	G	A	missense_variant c.98G>A p.Gly33Asp	ACP6EQ_09000	1,2-phenylacetyl-CoA epoxidase subunit PaaA

528

529 **Table S1: Assembly summary of NIH isolates**

Isolates	Contigs	Total length (>= 1000 bp)	N50	GC%	final contigs	Complete-ness	Contami-nation
NIH-010-1	154	6778138	81366	67.73	154	98.28	20.69
NIH-025-2	217	6917134	64404	67.59	213	98.28	10.34
NIH-010-2	213	6846762	60225	67.83	213	99.07	9.03
NIH-011-1	146	6714695	95958	67.77	146	99.53	7.94
NIH-018-3	141	6627574	94107	67.67	140	98.91	7.48
NIH-010-5	228	6582611	65494	67.7	202	98.28	6.9
NIH-027-1	157	7057208	92623	67.21	155	99.53	6.72
NIH-025-7	122	6736063	115055	67.59	122	99.07	6.23
NIH-013-1	264	7399130	58598	67.02	228	96.6	5.92
NIH-016-1	153	6938110	78345	67.68	152	99.24	5.61
NIH-015-1	219	7317467	69494	67.28	216	98.83	5.14
NIH-025-3	196	6971644	74558	67.55	196	99.3	4.21
NIH-016-3	162	6722923	73552	67.69	160	98.83	3.8
NIH-010-6	256	6589334	50077	67.69	254	99.51	3.27
NIH-010-4	183	6479449	67420	67.86	181	99.07	2.34
NIH-025-5	205	6816549	58213	67.6	201	98.95	2.02
NIH-016-2	97	6559927	124621	67.7	96	99.07	0.93
NIH-019-1	206	6967103	77893	68.34	203	99.53	0.93
NIH-022-1	129	6820766	102549	67.49	129	99.53	0.93
NIH-023-1	177	6736346	88615	67.51	175	99.53	0.93
NIH-003-1	122	6878569	94819	67.45	122	99.53	0.47
NIH-005-2	141	6466110	94875	67.79	141	99.53	0.47
NIH-005-3	106	6463122	116154	67.78	105	99.53	0.47
NIH-005-4	121	6727683	100896	67.65	119	99.53	0.47
NIH-009-1	75	6394470	194428	67.93	75	99.53	0.47
NIH-010-3	118	6438604	106660	67.83	118	99.07	0.47
NIH-014-1	97	6725191	135687	67.58	96	99.53	0.47
NIH-017-1	108	6968984	120623	67.49	107	99.3	0.47
NIH-018-1	143	6396229	81941	67.72	143	99.07	0.47
NIH-018-2	71	6407776	164746	67.72	71	99.53	0.47
NIH-025-1	138	6742034	90224	67.63	138	99.3	0.47
NIH-025-4	184	6682543	67033	67.58	184	98.6	0.47
NIH-025-6	181	6608399	67916	67.63	181	99.14	0.47
NIH-026-1	82	6375104	159180	67.87	81	99.07	0.47

NIH-021-1	118	6330035	97448	67.71	118	99.53	0

Table S2: Assembly summary of NCBI isolates

	Isolates	Completeness	Contamination
1	GCA_001641525_1	100	2.57
2	GCA_000165835_1	99.53	0.03
3	GCA_000508285_1	99.53	0.58
4	GCA_000967095_1	99.53	0.93
5	GCA_001038045_1	99.53	0.47
6	GCA_001276315_1	99.53	1.05
7	GCA_001457475_1	99.53	0.58
8	GCA_001471535_2	99.53	2.73
9	GCA_001541435_1	99.53	0.47
10	GCA_001558755_2	99.53	0
11	GCA_001559195_2	99.53	0.47
12	GCA_001566985_1	99.53	0.7
13	GCA_001598595_1	99.53	0.58
14	GCA_001654705_1	99.53	0.47
15	GCA_001707485_1	99.53	0
16	GCA_001810925_1	99.53	0.47
17	GCA_001957055_1	99.53	0.47
18	GCA_001957065_1	99.53	0.93
19	GCA_002083165_2	99.53	0.93
20	GCA_003031105_1	99.53	0.47
21	GCA_003177325_1	99.53	0.58
22	GCA_003293615_1	99.53	0.47
23	GCA_003503255_1	99.53	0
24	GCA_008432465_1	99.53	0.47
25	GCA_008631215_1	99.53	0.93
26	GCA_009363015_1	99.53	0.47
27	GCA_013282235_1	99.53	0.47
28	GCA_013282255_1	99.53	0.47
29	GCA_013343135_1	99.53	0.58
30	GCA_013413495_1	99.53	0.58
31	GCA_014353695_1	99.53	0
32	GCA_014529725_1	99.53	0
33	GCA_016403305_1	99.53	0.47
34	GCA_016599195_1	99.53	0.47
35	GCA_017745625_1	99.53	0
36	GCA_022320945_1	99.53	0.47
37	GCA_022320975_1	99.53	0.47
38	GCA_022321005_1	99.53	0.47

39	GCA_022321065_1	99.53	0.47
40	GCA_022321165_1	99.53	0.47
41	GCA_022321185_1	99.53	0.58
42	GCA_022321275_1	99.53	0.47
43	GCA_022321345_1	99.53	0.47
44	GCA_022325135_1	99.53	0.47
45	GCA_022325165_1	99.53	0.47
46	GCA_022325205_1	99.53	0.47
47	GCA_022444285_1	99.53	0.58
48	GCA_022488545_1	99.53	0.58
49	GCA_022524565_1	99.53	0.47
50	GCA_022524575_1	99.53	0.93
51	GCA_022524705_1	99.53	0.93
52	GCA_022524775_1	99.53	0.93
53	GCA_022524865_1	99.53	0.93
54	GCA_022525145_1	99.53	0.53
55	GCA_022525265_1	99.53	0.93
56	GCA_022525445_1	99.53	0.47
57	GCA_022976495_1	99.53	0.47
58	GCA_022976515_1	99.53	0.47
59	GCA_023703405_1	99.53	0.58
60	GCA_025426095_1	99.53	0.47
61	GCA_027529565_1	99.53	0.47
62	GCA_027529585_1	99.53	0.47
63	GCA_027529805_1	99.53	0.47
64	GCA_027529815_1	99.53	0.7
65	GCA_027922385_1	99.53	0.47
66	GCA_028462445_1	99.53	0.47
67	GCA_031994865_1	99.53	0.47
68	GCA_032703345_1	99.53	0.47
69	GCA_033096405_1	99.53	0.93
70	GCA_034424885_1	99.53	0.58
71	GCA_034424905_1	99.53	0.58
72	GCA_034424925_1	99.53	0.58
73	GCA_036035015_1	99.53	0.47
74	GCA_038277405_1	99.53	0
75	GCA_039595975_1	99.53	0.47
76	GCA_039674625_1	99.53	0.47
77	GCA_040438975_1	99.53	0.93
78	GCA_900009115_1	99.53	0.47
79	GCA_900009125_1	99.53	1.4
80	GCA_900010105_1	99.53	1.4

81	GCA_900475575_1	99.53	0.58
82	GCA_902363095_1	99.53	0.47
83	GCA_904067195_1	99.53	0.78
84	GCA_904067205_1	99.53	0.47
85	GCA_904067255_1	99.53	0.47
86	GCA_904067265_1	99.53	0.47
87	GCA_904067315_1	99.53	0.47
88	GCA_904067355_1	99.53	0.47
89	GCA_904067375_1	99.53	0.47
90	GCA_904067385_1	99.53	0.47
91	GCA_963528385_1	99.53	0.27
92	GCA_036527295_1	99.47	0.47
93	GCA_014490035_1	99.44	0
94	GCA_001299195_1	99.38	0
95	GCA_001299215_1	99.38	0.47
96	GCA_001558915_2	99.38	0.12
97	GCA_016027035_1	99.38	0.58
98	GCA_016728825_1	99.38	0.47
99	GCA_022870085_1	99.38	0.58
100	GCA_001299115_1	99.3	0.47
101	GCA_001299295_1	99.3	0.47
102	GCA_002192695_1	99.3	0
103	GCA_022321095_1	99.3	0.47
104	GCA_022325265_1	99.3	0.47
105	GCA_001299175_1	99.14	0.47
106	GCA_000517225_1	99.07	0.58
107	GCA_001051055_1	99.07	0
108	GCA_001298915_1	99.07	0.47
109	GCA_001957045_1	99.07	0.7
110	GCA_034078005_1	99.07	0.47
111	GCA_038024235_1	99.03	0
112	GCA_001299155_1	98.91	0.47
113	GCA_001815425_1	98.88	0.47
114	GCA_001299235_1	98.87	0.47
115	GCA_001298895_1	98.86	0.47
116	GCA_001299055_1	98.83	0.47
117	GCA_029837755_1	98.75	0.47
118	GCA_001299095_1	98.71	0.47
119	GCA_001298935_1	98.68	0.47
120	GCA_001299015_1	98.68	0.47
121	GCA_001299035_1	98.68	0.58
122	GCA_001299265_1	98.61	0.47

123	GCA_001299415_1	98.6	0.93
124	GCA_001813885_1	98.6	0.47
125	GCA_002294075_1	98.6	0.47
126	GCA_029837835_1	98.6	0.47
127	GCA_001298795_1	98.12	0
128	GCA_001299335_1	97.27	0.93
129	GCA_038024685_1	97.16	0
130	GCA_038024655_1	96.74	0.47
131	GCA_038024675_1	96.1	0.7
132	GCA_038024665_1	96.05	0.47
133	GCA_002453655_1	95.5	0.93
134	GCA_038024245_1	95.18	0.47
135	GCA_038024645_1	94.52	0
136	GCA_000186185_1	94.07	1.4
137	GCA_038049895_1	92.4	0
138	GCA_038049885_1	85.98	0.55
139	GCA_038049905_1	80.12	0.96
140	GCA_946222735_1	70.53	0
141	GCA_040396375_1	65.86	0

557 **Table S3: Antibiotic susceptibility testing for NIH clinical isolates with IMI and IMR.** R:
558 resistance. S: susceptible. I: intermediate resistance.

De-ID	Source	IMI MIC (mg/L)	interpretation	IMR MIC (mg/L)	Interpretation
NIH-003-1	Wound	<=1	S	2	S
NIH-005-2	Perirectal	2	S	4	I^
NIH-005-3	BAL	2	S	4	I^
NIH-005-4	Sputum	<=1	S	2	S
NIH-009-1	BAL	4	S	4	I^
NIH-010-1	Sputum	2	S	4	I^
NIH-010-2	Sputum	2	S	2	S
NIH-010-3	Sputum	2	S	2	S
NIH-010-4	BAL	2	S	2	S
NIH-010-5	Sputum	4	S	2	S
NIH-010-6	Skinlesion(mouth)	<=1	S	1	S
NIH-011-1	Sputum	<=1	S	1	S
NIH-013-1	BAL	<=1	S	2	S
NIH-014-1	AXL	<=1	S	2	S
NIH-015-1	Blood	<=1	S	1	S
NIH-016-1	Sputum	>8	R	>16	R
NIH-016-2	Sputum	4	S	4	I^
NIH-016-3	Sputum	>8	R	16	R
NIH-017-1	Nephrostomy urine	<=1	S	1	S
NIH-018-1	Sputum	<=1	S	2	S
NIH-018-2	Sputum	2	S	2	S
NIH-018-3	BAL	2	S	2	S
NIH-019-1	Sinus	2	S	2	S
NIH-021-1	wound	2	S	1	S
NIH-022-1	Sputum	4	S	4	I^
NIH-023-1	BAL	2	S	2	S
NIH-025-1	Blood	>8	R	8	R
NIH-025-2	Blood	>8	R	8	R
NIH-025-3	Blood	>8	R	8	R
NIH-025-4	axl	>8	R	8	R
NIH-025-5	Blood	>8	R	4	I^
NIH-025-6	BAL	>8	R	8	R
NIH-025-7	Blood	>8	R	4	I^
NIH-026-1	Wound (l heel)	4	S	2	S

559
560

561 ## 5. Discussion

562 *A. xylosoxidans* is an emerging pathogen that has garnered increasing attention in recent
563 years. Accurate identification of *Achromobacter* species has been challenging due to limited
564 knowledge, reliance on traditional and labor-intensive phenotypic identification methods, and
565 the lack of comprehensive spectra from representative species within MALDI-TOF databases
566 (74). Advances in sequencing technology and the decreasing cost of sequencing have made
567 whole genome sequencing a feasible approach for identifying *A. xylosoxidans*. Mining these
568 whole genome sequencing data can provide insights into the genetic diversity, antibiotic
569 resistance mechanisms, and virulence potential of these isolates. In this study, we analyzed
570 publicly available sequences from NCBI and our data from isolates collected at the NIH clinical
571 centers representing various genetic backgrounds.

572

573 Our core genome analysis revealed that *A. xylosoxidans* possesses a relatively small core
574 genome (less than 60% of its total genes). This is smaller than the core genomes of other
575 opportunistic pathogens such as *P. aeruginosa* and *Helicobacter pylori*. For instance, *P.*
576 *aeruginosa* has approximately 5,300 core genes (75) out of a total of ~ 5,700 genes (76),
577 accounting for more than 92% of its genome. Similarly, *Helicobacter pylori* has 1,227 core
578 genes (77) out of ~1,500 total genes (78), making up 81% of its genome. The core genome
579 phylogenetic tree of *A. xylosoxidans* appears to be non-clonal and isolates from the same
580 geographic locations or sample sources did not cluster together. The lack of population
581 structure and co-ancestry suggests that *A. xylosoxidans* isolates are likely evolving
582 independently, possibly under selective pressures in different environments or hosts. Such
583 variations may arise from diverse soil or water environments (where *Achromobacter* are
584 usually found), or from differences in antibiotics treatment regimens, underlying host
585 diseases, or other health conditions. It is also worth noting that we do observe an exception
586 of a few environmental isolates that do show some level of shared ancestry. Most isolates
587 collected from the same patients clustered together and shared co-ancestry (Figures 2 and
588 S1) suggesting that they evolved from the same infection. However, an exception was
589 observed with NIH-005-4, which did not cluster with NIH-005-3 and NIH-005-2, indicating that
590 NIH-005-2 and NIH-005-3 likely represent a case of reinfection rather than a persistent
591 infection.

592

593 The multidrug resistance of *A. xylosoxidans* is common and concerning (Figure 3). This
594 bacterium encodes several efflux pumps, although a few have been validated. The resistance-
595 nodulation-cell division (RND)-type multidrug efflux pump, AxyABM, gave some level of
596 resistant to cephalosporins (except cefepime), aztreonam, nalidicic acid, fluoroquinolones and
597 chloramphenicol (79). Recently, a novel RND-type multidrug efflux pump, AxyXY-OprZ, was
598 identified, which expels antibiotics such as cefepime, fluoroquinolones, tetracycline or

599 aminoglycosides including kanamycin, gentamicin, and tobramycin (80). Additionally, a recent
600 study discovered the presence of another narrow-spectrum RND-type multidrug efflux pump,
601 AxyEF-OprN, which pumps out fluoroquinolones, tetracyclines, and carbapenems (31).
602 Furthermore, a very recent study identified AxySUV in some of the *A. xylosoxidans* genomes
603 that export fluoroquinolones (ciprofloxacin, levofloxacin), carbapenems (doripenem),
604 tetracycline (doxycycline, minocycline), and chloramphenicol (81). In addition to the presence
605 of various efflux pumps, intrahost evolution may contribute to increasing antibiotic resistance
606 over time. One interesting case is the NIH-016 series. NIH-016-3, collected seven months after
607 NIH-016-2 from the same patient, exhibits higher AR and enhanced biofilm formation
608 compared to NIH-016-2. Phylogenetic analysis confirms their close relationship, suggesting
609 that NIH-016-3 evolved from NIH-016-2. While both isolates carry similar sets of resistance
610 genes identified from the CARD database, NIH-016-3 demonstrates greater resistance to
611 antibiotics. Comparing single nucleotide polymorphism of all three isolates in the series
612 suggest that the later collected isolates accumulated mutations in the efflux pump (AxyXY-
613 OprZ) and DNA mismatch repair systems that could facilitate the adaptation of the isolates to
614 antibiotic treatment. Further study is needed to validate the roles of these SNPs.

615 In our NIH isolates, 21% of isolates are resistant to IMI while 34% isolates are resistant to IMR.
616 Our models predict 20% resistant to IMR among NCBI isolates. Relebactam, a wide spectrum
617 β – lactamase inhibitor against class A (extended spectrum β–lactamases KPC) and class C
618 (AmpC) β–lactamases, does not seem to work in *Achromobacter*. In fact, all NIH isolates that
619 were resistant to IMI were also resistant to IMR (Table S3). In other bacteria such as
620 *Pseudomonas* and *Klebsiella*, IMR was more effective than IMI (82, 83). This could be because
621 *A. xylosoxidans* possesses other β–lactamases classes. NIH-016s possess AXC family
622 carbapenem-hydrolyzing class A β–lactamase and OXA-114 family class D β–lactamase. The
623 OXA-114 may help *Achromobacter* to escape relebactam. These findings highlight that *A.*
624 *xylosoxidans* employ multiple AR genes and strategies, which require further research .

625

626 As secretion systems are key virulent factors in bacteria, we investigated the presence of all
627 possible secretion systems in the NIH isolates. T1SS, T2SS, T5SS, and bacterial Tight adherence
628 Secretion System (TadSS) were identified in all isolates. T1SS is capable of transporting
629 unfolded substrates, including digestive enzymes (proteases and lipases), adhesins, heme-
630 binding proteins, and proteins with repeats-in-toxins (RTX) motifs (84). T2SS, a secretion
631 machinery prevalent in many Gram-negative bacteria, facilitates the secretion of virulence
632 factors such as proteases, toxins, lipases, and carbohydrate-degrading enzymes, which aid the
633 survival of both pathogenic and environmental bacteria (85). T5SS is involved in the secretion
634 of virulence proteins critical to pathogenesis in several bacteria, including immunoglobulin A
635 protease of *Neisseria gonorrhoeae (86)*, IcsA protein of *Shigella flexneri* (87), and YadA of
636 *Yersinia enterocolitica (88)*. TadSS is an important secretion system that supports infection,
637 cell adherence, competence, and biofilm formation in many pathogenic bacteria, such as *P.*

638 *aeruginosa*, *Bordetella pertussis*, *Burkholderia pseudomallei*, and *Mycobacterium tuberculosis*
639 (89). The presence of these secretion systems in all isolates suggests that they all have the
640 potential to be pathogenic.

641 Most isolates have T3SS, T4SS, T6SS and flagella. T3SS is associated with the cytotoxicity of
642 the isolates (15). AxoU is the only known T3SS substrate that is responsible for host cell
643 cytotoxicity in *A. xylosoxidans*. All cytotoxic isolates carried both T3SS and AxoU, except NIH-
644 019-1 carries T3SS but not AxoU, suggesting the presence of unidentified T3SS substrate(s).
645 T4SS is primarily involved in horizontal genetic transfer (HGT) between different
646 microorganisms, which may contribute to pathogenesis and antibiotic resistance (16). T6SS is
647 a multiprotein complex that uses a spring-like mechanism to deliver effector proteins into
648 target cells (90). In *A. xylosoxidans,* T6SS plays a role in targeting competing bacteria and is
649 crucial for the internalization of the pathogen into lung epithelial cells (16). Flagella, which are
650 evolutionarily related to T3SS, play roles in motility, surface adherence and biofilm formation
651 (91). Interestingly, while most isolates encode flagellar genes, only 59% of them are motile,
652 suggesting an adaptation strategy of the chronic infection isolates. A study on the genotypic
653 and phenotypic evolution of the *A.xylosoxidans* isolates collected from CF patients over time
654 showed a decrease in swimming motility, an increase in antibiotic resistance, and enhanced
655 biofilm formation in evolved strains (92).

656

657 Phylogenetic analysis indicates that the T3SS of *A. xylosoxidans* structurally belongs to the Ysc
658 family of T3SS systems, which includes *Bordetella* spp. (alpha-proteobacteria), *Yersinia* spp.,
659 *P. aeruginosa*, *Aeromonas* spp., *Photorhabdus luminescens*, and *Vibrio* spp. (gamma-
660 proteobacteria) (Figure 4). In *Bordetella spp*., *Yersinia* spp., and *Photorhabdus luminescens,*
661 the T3SS confers resistance to the innate immune response by inhibiting phagocytosis, leading
662 to extracellular localization of the pathogens (93-95). While *P. aeruginosa* is known as an
663 extracellular pathogen, it can replicate intracellularly where T3SS and its effectors (mainly
664 ExoS) play critical roles in internalization, vacuole escape, evasion of inflammasome and
665 autophagy as well as bleb formation prior to detachment (96). Similarly, T3SS is important for
666 *Aeromonas* and *Vibrio* to maintain its intracellular niches (97, 98). In *A. xylosoxidans,* survival
667 within macrophages for several hours is independent of T3SS; however, cytotoxicity depends
668 on the presence of T3SS (12, 13). AxoU is the only known T3SS substrate linked to host cell
669 lysis (15), although other T3SS effectors may be secreted during infection, as disrupting the
670 T3SS (e.g., *sctV*) prevents cell death, whereas disruption of *axoU* alone does not (12).
671 Interestingly, T3SS and *axoU* are expressed shortly after infection (within 30 minutes), but are
672 subsequently turned off (12). Whether T3SS is reactivated when the bacteria escape the
673 vacuole and lyse the host cells remain to be tested. Whether there exist additional T3SS
674 effectors and what their roles are require further study.

675 Cytotoxicity demonstrates substantial heterogeneity among our clinical isolates (Figure 5). *A.*
676 *xylosoxidans* cytotoxicity is conducted through its T3SS with the major effector known to

677 cause cell death being AxoU, a homologue of ExoU found in *P. aeruginosa (99).* Interestingly,
678 our results would imply the presence of at least one additional effector which contributes to
679 cytotoxicity. While lacking *axoU* on its chromosome, NIH-019-1 demonstrated significantly
680 increased cytotoxicity compared to the GN008 negative control. The expression of T3SS only
681 occurs following phagocytosis and is not contact-dependent (13). There was no observable
682 relationship between overall flagellar motility and cytotoxicity but a small association with
683 biofilm production and cytotoxicity (Figure S2). In NIH-018 series, there was an increase in
684 cytotoxicity from isolates collected after the others (Table 2). This is interesting, as in other
685 bacteria, the bacteria tend to get less virulent when they colonized the host for a long time
686 (100, 101) .

687

688 Biofilm production is another major aspect of the bacterial lifestyle. Production of biofilm is
689 important in promoting bacterial resistance to environmental pressures and defending against
690 immune cells during infection. The NIH isolates produce low level of biofilm in general (Figure
691 6). We observed a slight increase in biofilm production in the intrahost isolates, NIH-010s, NIH-
692 016s and NIH-018s but it is not significant. GN050 collected from ear effusion (15), is the only
693 isolate that produced robust biofilm. It could be that because most of our isolates were from
694 respiratory tract, they don't form as much biofilm. Alternatively, biofilm was tightly regulated,
695 and we didn't assay the bacteria in the desire condition for biofilm formation in these
696 particular isolates. Biofilm production was not correlated with motility (Figure S2), although
697 the strong biofilm former are moderately motile. Biofilm was not correlated with antibiotic
698 resistance, indicating these phenotypes operate through independent mechanisms.

699

700 Flagellar motility in bacteria is commonly associated with increased disease severity and
701 pathogenesis. Multiple related species such as *Bordetella* and *Pseudomonas* are known to
702 have the expression of virulence systems such as the T3SS modulated by the expression of the
703 flagella (65, 102) . Additionally, bacteria with dysfunctional flagella are known to have reduced
704 pathogenicity *in vivo* due to the inability to reach the site of infection (64). Bacteria isolated
705 from the lungs are known to preferentially gain mutations in the flagella resulting in non-
706 motile genotypes as compared to other sites of infection (60) (66). Our results demonstrated
707 this trend. We identified a mutation in *fliF* which we could result in a loss of flagellar
708 production. We observed no correlation between overall motility and cytotoxicity (Figure S2).
709 Interestingly, isolates that are the most cytotoxic are motile, but the most motile isolates are
710 not cytotoxic. It could be possible that the most motile isolates can escape phagocytosis in
711 our *invitro* infection. Strains that experience a loss of either flagellar motility or cytotoxicity
712 do not experience a relative loss in the other. It is unclear what role the flagella of *A.*
713 *xylosoxidans* plays during infection. In multiple bacteria species the function of the flagella is
714 highly correlated with the activity of virulence mechanisms. The regulatory relationship
715 between motility and virulence varies substantially between organisms. *Bordetella spp.*

716 display an inverse relationship (102), whereas *Pseudomonas aeruginosa* displays a positive
717 relationship between T3SS production and flagellar motility (65). *Salmonella spp.* also
718 demonstrate a positive relationship with the SPI-1 T3SS but not the SPI-2 T3SS (103). These
719 observations indicate a general positive correlation between flagella and virulence factor
720 expression in extracellular pathogens. In *A. xylosoxidans,* T3SS expression seemed to increase
721 shortly after the bacteria are phagocytosed by macrophage but dampened quickly. Whether
722 T3SS is shut off and then gets re-activated at later stage of infection or it remains functional
723 to some extend without making more apparatus and elevated level of substrate production
724 requires further investigations.

725

726 In summary, this study highlights the genetic and phenotypic diversity among *A. xylosoxidans*
727 isolates, as evidenced by the high accessory genome content and variability in secretion
728 systems. Significant differences in antibiotic resistance and virulence mechanisms underscore
729 the adaptability of this bacterial species. These findings emphasize the need for further
730 mechanistic studies to elucidate the pathogenicity and antibiotic resistance mechanisms of *A.*
731 *xylosoxidans*.

732

733

734

735 ## 6. Author statements

736 Pooja Acharya (Formal Analysis, Data Curation, Methodology, Writing), Cameron Lloyd
737 (Formal Analysis, Methodology, Writing), Ngoc Thien Lam (Formal Analysis, Writing), Jessica
738 Kumke (Formal Analysis), Sreejana Ray (Resources), Zilia Yanira Muñoz Ramirez (Formal
739 Analysis), Sanjay Mandal (Formal analysis), Sanchita Das (conceptualization, resources) and
740 Hanh Ngoc Lam (Conceptualization, Data Curation, Formal Analysis, Funding Acquisition,
741 Investigation, Methodology, Supervision, Writing)

742

743 ### 6.1 Conflicts of interest

744 *The author(s) declare that there are no conflicts of interest*

745 ### 6.2 Funding information

746 This work is supported by NIH R00AI139281.

747 ### 6.3 Acknowledgements

748 This work is supported by NIH R00AI139281.
749

750 ## 7. References

751 1. Veschetti L, Boaretti M, Saitta GM, Passarelli Mantovani R, Lleo MM, Sandri A, et al.
752 Achromobacter spp. prevalence and adaptation in cystic fibrosis lung infection. Microbiol
753 Res. 2022;263:127140.
754 2. Jeukens J, Freschi L, Vincent AT, Emond-Rheault JG, Kukavica-Ibrulj I, Charette SJ, et
755 al. A Pan-Genomic Approach to Understand the Basis of Host Adaptation in Achromobacter.
756 Genome Biol Evol. 2017;9(4):1030-46.
757 3. Yabuuchi E, Oyama A. Achromobacter xylosoxidans n. sp. from human ear discharge.
758 Jpn J Microbiol. 1971;15(5):477-81.
759 4. Swenson CE, Sadikot RT. Achromobacter respiratory infections. Ann Am Thorac Soc.
760 2015;12:252-8.
761 5. Jakobsen TH, Hansen MA, Jensen PØ, Hansen L, Riber L, Cockburn A, et al. Complete
762 Genome Sequence of the Cystic Fibrosis Pathogen Achromobacter xylosoxidans NH44784-
763 1996 Complies with Important Pathogenic Phenotypes. PLoS ONE. 2013;8(7):e68484.
764 6. Esposito S, Pisi G, Fainardi V, Principi N. What is the role of Achromobacter species in
765 patients with cystic fibrosis? Front Biosci (Landmark Ed). 2021;26(12):1613-20.
766 7. Tetart M, Wallet F, Kyheng M, Leroy S, Perez T, Le Rouzic O, et al. Impact of
767 Achromobacter xylosoxidans isolation on the respiratory function of adult patients with
768 cystic fibrosis. ERJ Open Res. 2019;5(4).
769 8. Somayaji R, Stanojevic S, Tullis DE, Stephenson AL, Ratjen F, Waters V. Clinical
770 Outcomes Associated with Achromobacter Species Infection in Patients with Cystic Fibrosis.
771 Ann Am Thorac Soc. 2017;14(9):1412-8.
772 9. Nielsen SM, Penstoft LN, Nørskov-Lauritsen N. Motility, Biofilm Formation and
773 Antimicrobial Efflux of Sessile and Planktonic Cells of Achromobacter xylosoxidans.
774 Pathogens. 2019;8(1):14.
775 10. Li X, Hu Y, Gong J, Zhang L, Wang G. Comparative genome characterization of
776 Achromobacter members reveals potential genetic determinants facilitating the adaptation
777 to a pathogenic lifestyle. Applied Microbiology and Biotechnology. 2013;97(14):6413-25.
778 11. Wills BM, Garai P, Riegert MO, Sanchez FT, Pickrum AM, Frank DW, et al.
779 Identification of Virulence Factors Involved in a Murine Model of Severe Achromobacter
780 xylosoxidans Infection. Infect Immun. 2023;91(7):e0003723.
781 12. Turton K, Parks HJ, Zarodkiewicz P, Hamad MA, Dwane R, Parau G, et al. The
782 Achromobacter type 3 secretion system drives pyroptosis and immunopathology via
783 independent activation of NLRC4 and NLRP3 inflammasomes. Cell Rep. 2023;42(8):113012.
784 13. Pickrum AM, Riegert MO, Wells C, Brockman K, Frank DW. The In Vitro Replication
785 Cycle of Achromobacter xylosoxidans and Identification of Virulence Genes Associated with
786 Cytotoxicity in Macrophages. Microbiol Spectr. 2022;10(4):e0208322.
787 14. Li X, Hu Y, Gong J, Zhang L, Wang G. Comparative genome characterization of
788 Achromobacter members reveals potential genetic determinants facilitating the adaptation
789 to a pathogenic lifestyle. Appl Microbiol Biotechnol. 2013;97(14):6413-25.
790 15. Pickrum AM, DeLeon O, Dirck A, Tessmer MH, Riegert MO, Biller JA, et al.
791 Achromobacter xylosoxidans Cellular Pathology Is Correlated with Activation of a Type III
792 Secretion System. Infect Immun. 2020;88(7).
793 16. Le Goff M, Vastel M, Lebrun R, Mansuelle P, Diarra A, Grandjean T, et al.
794 Characterization of the Achromobacter xylosoxidans Type VI Secretion System and Its
795 Implication in Cystic Fibrosis. Front Cell Infect Microbiol. 2022;12:859181.

17. Troisfontaines P, Cornelis GR. Type III secretion: more systems than you think. Physiology (Bethesda). 2005;20:326-39.
18. Weyrich LS, Rolin OY, Muse SJ, Park J, Spidale N, Kennett MJ, et al. A Type VI secretion system encoding locus is required for Bordetella bronchiseptica immunomodulation and persistence in vivo. PLoS One. 2012;7(10):e45892.
19. Nolan LM, Allsopp LP. Antimicrobial Weapons of Pseudomonas aeruginosa. Adv Exp Med Biol. 2022;1386:223-56.
20. Aggarwal S, Garcia-Telles N, Aggarwal G, Lavie C, Lippi G, Henry BM. Clinical features, laboratory characteristics, and outcomes of patients hospitalized with coronavirus disease 2019 (COVID-19): Early report from the United States. Diagnosis (Berl). 2020;7(2):91-6.
21. Lorenz A, Preusse M, Bruchmann S, Pawar V, Grahl N, Pils MC, et al. Importance of flagella in acute and chronic Pseudomonas aeruginosa infections. Environ Microbiol. 2019;21(3):883-97.
22. Isler B, Kidd TJ, Stewart AG, Harris P, Paterson DL. Achromobacter Infections and Treatment Options. Antimicrob Agents Chemother. 2020;64(11).
23. Swenson CE, Sadikot RT. Achromobacter respiratory infections. Ann Am Thorac Soc. 2015;12(2):252-8.
24. Hu Y, Zhu Y, Ma Y, Liu F, Lu N, Yang X, et al. Genomic insights into intrinsic and acquired drug resistance mechanisms in Achromobacter xylosoxidans. Antimicrob Agents Chemother. 2015;59(2):1152-61.
25. Sakagianni A, Koufopoulou C, Feretzakis G, Kalles D, Verykios VS, Myrianthefs P, et al. Using Machine Learning to Predict Antimicrobial Resistance-A Literature Review. Antibiotics (Basel). 2023;12(3).
26. Khaledi A, Weimann A, Schniederjans M, Asgari E, Kuo TH, Oliver A, et al. Predicting antimicrobial resistance in Pseudomonas aeruginosa with machine learning-enabled molecular diagnostics. EMBO Mol Med. 2020;12(3):e10264.
27. Hyun JC, Kavvas ES, Monk JM, Palsson BO. Machine learning with random subspace ensembles identifies antimicrobial resistance determinants from pan-genomes of three pathogens. PLoS Comput Biol. 2020;16(3):e1007608.
28. Kavvas ES, Catoiu E, Mih N, Yurkovich JT, Seif Y, Dillon N, et al. Machine learning and structural analysis of Mycobacterium tuberculosis pan-genome identifies genetic signatures of antibiotic resistance. Nat Commun. 2018;9(1):4306.
29. Nguyen M, Long SW, McDermott PF, Olsen RJ, Olson R, Stevens RL, et al. Using Machine Learning To Predict Antimicrobial MICs and Associated Genomic Features for Nontyphoidal Salmonella. J Clin Microbiol. 2019;57(2).
30. Yan J, Bassler BL. Surviving as a Community: Antibiotic Tolerance and Persistence in Bacterial Biofilms. Cell Host Microbe. 2019;26(1):15-21.
31. Nielsen SM, Penstoft LN, Norskov-Lauritsen N. Motility, Biofilm Formation and Antimicrobial Efflux of Sessile and Planktonic Cells of Achromobacter xylosoxidans. Pathogens. 2019;8(1).
32. Bolger AM, Lohse M, Usadel B. Trimmomatic: a flexible trimmer for Illumina sequence data. Bioinformatics. 2014;30(15):2114-20.
33. Andrews S. FastQC: a quality control tool for high throughput sequence data. 2010.
34. Bankevich A, Nurk S, Antipov D, Gurevich AA, Dvorkin M, Kulikov AS, et al. SPAdes: a new genome assembly algorithm and its applications to single-cell sequencing. J Comput Biol. 2012;19(5):455-77.

35. Gurevich A, Saveliev V, Vyahhi N, Tesler G. QUAST: quality assessment tool for genome assemblies. Bioinformatics. 2013;29(8):1072-5.
36. Parks DH, Imelfort M, Skennerton CT, Hugenholtz P, Tyson GW. CheckM: assessing the quality of microbial genomes recovered from isolates, single cells, and metagenomes. Genome Res. 2015;25(7):1043-55.
37. Seemann T. Prokka: rapid prokaryotic genome annotation. Bioinformatics. 2014;30(14):2068-9.
38. Tonkin-Hill G, MacAlasdair N, Ruis C, Weimann A, Horesh G, Lees JA, et al. Producing polished prokaryotic pangenomes with the Panaroo pipeline. Genome Biol. 2020;21(1):180.
39. Hall BG, Nisbet J. Building Phylogenetic Trees From Genome Sequences With kSNP4. Mol Biol Evol. 2023;40(11).
40. Stamatakis A. RAxML version 8: a tool for phylogenetic analysis and post-analysis of large phylogenies. Bioinformatics. 2014;30(9):1312-3.
41. Letunic I, Bork P. Interactive Tree of Life (iTOL) v6: recent updates to the phylogenetic tree display and annotation tool. Nucleic Acids Res. 2024;52(W1):W78-W82.
42. Yahara K, Didelot X, Ansari MA, Sheppard SK, Falush D. Efficient inference of recombination hot regions in bacterial genomes. Mol Biol Evol. 2014;31(6):1593-605.
43. Browning BL, Browning SR. A unified approach to genotype imputation and haplotype-phase inference for large data sets of trios and unrelated individuals. Am J Hum Genet. 2009;84(2):210-23.
44. Lawson DJ, Hellenthal G, Myers S, Falush D. Inference of population structure using dense haplotype data. PLoS Genet. 2012;8(1):e1002453.
45. Yahara K, Furuta Y, Oshima K, Yoshida M, Azuma T, Hattori M, et al. Chromosome painting in silico in a bacterial species reveals fine population structure. Mol Biol Evol. 2013;30(6):1454-64.
46. Abby SS, Cury J, Guglielmini J, Neron B, Touchon M, Rocha EP. Identification of protein secretion systems in bacterial genomes. Sci Rep. 2016;6:23080.
47. Katoh K, Standley DM. MAFFT multiple sequence alignment software version 7: improvements in performance and usability. Mol Biol Evol. 2013;30(4):772-80.
48. Kokot M, Dlugosz M, Deorowicz S. KMC 3: counting and manipulating k-mer statistics. Bioinformatics. 2017;33(17):2759-61.
49. Pedregosa F, Varoquaux G, Gramfort A, Michel V, Thirion B, Grisel O, et al. Scikit-learn: Machine learning in Python. the Journal of machine Learning research. 2011;12:2825-30.
50. Chen TQ, Guestrin C. XGBoost: A Scalable Tree Boosting System. Kdd'16: Proceedings of the 22nd Acm Sigkdd International Conference on Knowledge Discovery and Data Mining. 2016:785-94.
51. Ray S, Flemming LK, Scudder CJ, Ly MA, Porterfield HS, Smith RD, et al. Comparative phenotypic and genotypic antimicrobial susceptibility surveillance in Achromobacter spp. through whole genome sequencing. Microbiol Spectr. 2025;13(4):e0252724.
52. Kalantar KL, Carvalho T, de Bourcy CFA, Dimitrov B, Dingle G, Egger R, et al. IDseq-An open source cloud-based pipeline and analysis service for metagenomic pathogen detection and monitoring. Gigascience. 2020;9(10).
53. Bador J, Neuwirth C, Grangier N, Muniz M, Germe L, Bonnet J, et al. Role of AxyZ Transcriptional Regulator in Overproduction of AxyXY-OprZ Multidrug Efflux System in Achromobacter Species Mutants Selected by Tobramycin. Antimicrob Agents Chemother. 2017;61(8).

889 54. Rees VE, Deveson Lucas DS, Lopez-Causape C, Huang Y, Kotsimbos T, Bulitta JB, et al.
890 Characterization of Hypermutator Pseudomonas aeruginosa Isolates from Patients with
891 Cystic Fibrosis in Australia. Antimicrob Agents Chemother. 2019;63(4).
892 55. Veschetti L, Sandri A, Johansen HK, Lleo MM, Malerba G. Hypermutation as an
893 Evolutionary Mechanism for Achromobacter xylosoxidans in Cystic Fibrosis Lung Infection.
894 Pathogens. 2020;9(2).
895 56. Ragheb MN, Thomason MK, Hsu C, Nugent P, Gage J, Samadpour AN, et al. Inhibiting
896 the Evolution of Antibiotic Resistance. Mol Cell. 2019;73(1):157-65 e5.
897 57. Davidson AL, Chen J. ATP-binding cassette transporters in bacteria. Annu Rev
898 Biochem. 2004;73:241-68.
899 58. Chen L, Zou Y, She P, Wu Y. Composition, function, and regulation of T6SS in
900 Pseudomonas aeruginosa. Microbiol Res. 2015;172:19-25.
901 59. Warrier A, Satyamoorthy K, Murali TS. Quorum-sensing regulation of virulence
902 factors in bacterial biofilm. Future Microbiol. 2021;16:1003-21.
903 60. Holban AM, Gregoire CM, Gestal MC. Conquering the host: Bordetella spp. and
904 Pseudomonas aeruginosa molecular regulators in lung infection. Front Microbiol.
905 2022;13:983149.
906 61. Passos da Silva D, Matwichuk ML, Townsend DO, Reichhardt C, Lamba D, Wozniak DJ,
907 et al. The Pseudomonas aeruginosa lectin LecB binds to the exopolysaccharide Psl and
908 stabilizes the biofilm matrix. Nat Commun. 2019;10(1):2183.
909 62. Starkey M, Hickman JH, Ma L, Zhang N, De Long S, Hinz A, et al. Pseudomonas
910 aeruginosa rugose small-colony variants have adaptations that likely promote persistence in
911 the cystic fibrosis lung. J Bacteriol. 2009;191(11):3492-503.
912 63. Kazmierczak BI, Schniederberend M, Jain R. Cross-regulation of Pseudomonas
913 motility systems: the intimate relationship between flagella, pili and virulence. Curr Opin
914 Microbiol. 2015;28:78-82.
915 64. Feldman M, Bryan R, Rajan S, Scheffler L, Brunnert S, Tang H, et al. Role of flagella in
916 pathogenesis of Pseudomonas aeruginosa pulmonary infection. Infect Immun.
917 1998;66(1):43-51.
918 65. Soscia C, Hachani A, Bernadac A, Filloux A, Bleves S. Cross talk between type III
919 secretion and flagellar assembly systems in Pseudomonas aeruginosa. J Bacteriol.
920 2007;189(8):3124-32.
921 66. Planet PJ. Adaptation and Evolution of Pathogens in the Cystic Fibrosis Lung. J
922 Pediatric Infect Dis Soc. 2022;11(Supplement_2):S23-S31.
923 67. Schniederberend M, Abdurachim K, Murray TS, Kazmierczak BI. The GTPase activity
924 of FlhF is dispensable for flagellar localization, but not motility, in Pseudomonas aeruginosa.
925 J Bacteriol. 2013;195(5):1051-60.
926 68. Lloyd CJ, Klose KE. The Vibrio Polar Flagellum: Structure and Regulation. Adv Exp Med
927 Biol. 2023;1404:77-97.
928 69. Blum M, Andreeva A, Florentino LC, Chuguransky SR, Grego T, Hobbs E, et al.
929 InterPro: the protein sequence classification resource in 2025. Nucleic Acids Res.
930 2025;53(D1):D444-D56.
931 70. Bange G, Petzold G, Wild K, Parlitz RO, Sinning I. The crystal structure of the third
932 signal-recognition particle GTPase FlhF reveals a homodimer with bound GTP. Proc Natl Acad
933 Sci U S A. 2007;104(34):13621-5.

934 71. Zhang K, He J, Cantalano C, Guo Y, Liu J, Li C. FlhF regulates the number and
935 configuration of periplasmic flagella in Borrelia burgdorferi. Mol Microbiol.
936 2020;113(6):1122-39.
937 72. Balaban M, Joslin SN, Hendrixson DR. FlhF and its GTPase activity are required for
938 distinct processes in flagellar gene regulation and biosynthesis in Campylobacter jejuni. J
939 Bacteriol. 2009;191(21):6602-11.
940 73. Jumper J, Evans R, Pritzel A, Green T, Figurnov M, Ronneberger O, et al. Highly
941 accurate protein structure prediction with AlphaFold. Nature. 2021;596(7873):583-9.
942 74. Papalia M, Figueroa-Espinosa R, Steffanowski C, Barberis C, Almuzara M, Barrios R, et
943 al. Expansion and improvement of MALDI-TOF MS databases for accurate identification of
944 Achromobacter species. J Microbiol Methods. 2020;172:105889.
945 75. Ozer EA, Allen JP, Hauser AR. Characterization of the core and accessory genomes of
946 Pseudomonas aeruginosa using bioinformatic tools Spine and AGEnt. Bmc Genomics.
947 2014;15.
948 76. Klockgether J, Cramer N, Wiehlmann L, Davenport CF, Tummler B. Pseudomonas
949 aeruginosa Genomic Structure and Diversity. Front Microbiol. 2011;2:150.
950 77. Thorell K, Muñoz-Ramírez ZY, Wang D, Sandoval-Motta S, Boscolo Agostini R, Ghirotto
951 S, et al. The Helicobacter pylori Genome Project: insights into H. pylori population structure
952 from analysis of a worldwide collection of complete genomes. Nature Communications.
953 2023;14(1).
954 78. Salama NR, Shepherd B, Falkow S. Global transposon mutagenesis and essential gene
955 analysis of Helicobacter pylori. J Bacteriol. 2004;186(23):7926-35.
956 79. Bador J, Amoureux L, Duez J-M, Drabowicz A, Siebor E, Llanes C, et al. First
957 Description of an RND-Type Multidrug Efflux Pump in Achromobacter xylosoxidans, AxyABM.
958 Antimicrobial Agents and Chemotherapy. 2011;55(10):4912-4.
959 80. Bador J, Amoureux L, Blanc E, Neuwirth C. Innate Aminoglycoside Resistance of
960 Achromobacter xylosoxidans Is Due to AxyXY-OprZ, an RND-Type Multidrug Efflux Pump.
961 Antimicrobial Agents and Chemotherapy. 2013;57(1):603-5.
962 81. Magallon A, Bador J, Garrigos T, Demeule C, Chapelle A, Varin V, et al. Description of
963 Two Resistance-Nodulation-Cell Division Efflux Systems Involved in Acquired Antibiotic
964 Resistance: AxySUV in Achromobacter xylosoxidans and AinCDJ in Achromobacter insuavis.
965 Antibiotics (Basel). 2025;14(6).
966 82. Ventero MP, Haro-Moreno JM, Molina-Pardines C, Sanchez-Bautista A, Garcia-Rivera
967 C, Boix V, et al. Role of Relebactam in the Antibiotic Resistance Acquisition in Pseudomonas
968 aeruginosa: In Vitro Study. Antibiotics (Basel). 2023;12(11).
969 83. Palomba E, Comelli A, Saluzzo F, Di Marco F, Matarazzo E, Re NL, et al. Activity of
970 imipenem/relebactam against KPC-producing Klebsiella pneumoniae and the possible role of
971 Ompk36 mutation in determining resistance: an Italian retrospective analysis. Ann Clin
972 Microbiol Antimicrob. 2025;24(1):23.
973 84. Holland IB, Schmitt L, Young J. Type 1 protein secretion in bacteria, the ABC-
974 transporter dependent pathway (review). Mol Membr Biol. 2005;22(1-2):29-39.
975 85. Korotkov KV, Sandkvist M. Architecture, Function, and Substrates of the Type II
976 Secretion System. EcoSal Plus. 2019;8(2):227-44.
977 86. Pohlner J, Halter R, Meyer TF. Neisseria gonorrhoeae IgA protease. Secretion and
978 implications for pathogenesis. Antonie Van Leeuwenhoek. 1987;53(6):479-84.
979 87. Brandon LD, Goehring N, Janakiraman A, Yan AW, Wu T, Beckwith J, et al. IcsA, a
980 polarly localized autotransporter with an atypical signal peptide, uses the Sec apparatus for

secretion, although the Sec apparatus is circumferentially distributed. Mol Microbiol. 2003;50(1):45-60.
88. Roggenkamp A, Ackermann N, Jacobi CA, Truelzsch K, Hoffmann H, Heesemann J. Molecular analysis of transport and oligomerization of the Yersinia enterocolitica adhesin YadA. J Bacteriol. 2003;185(13):3735-44.
89. Tassinari M, Rudzite M, Filloux A, Low HH. Assembly mechanism of a Tad secretion system secretin-pilotin complex. Nature Communications. 2023;14(1).
90. Cherrak Y, Flaugnatti N, Durand E, Journet L, Cascales E. Structure and Activity of the Type VI Secretion System. Microbiology Spectrum. 2019;7(4):329-42.
91. Zhang X, Zeng W, Kong J, Huang Z, Shu H, Tang M, et al. The prevalence and mechanisms of heteroresistance to ceftazidime/avibactam in KPC-producing Klebsiella pneumoniae. J Antimicrob Chemother. 2024;79(8):1865-76.
92. Khademi SMH, Gabrielaite M, Paulsson M, Knulst M, Touriki E, Marvig RL, et al. Genomic and Phenotypic Evolution of Achromobacter xylosoxidans during Chronic Airway Infections of Patients with Cystic Fibrosis. mSystems. 2021;6(3).
93. Seabaugh JA, Anderson DM. Pathogenicity and virulence of Yersinia. Virulence. 2024;15(1):2316439.
94. Yuk MH, Harvill ET, Cotter PA, Miller JF. Modulation of host immune responses, induction of apoptosis and inhibition of NF-kappaB activation by the Bordetella type III secretion system. Mol Microbiol. 2000;35(5):991-1004.
95. Brugirard-Ricaud K, Duchaud E, Givaudan A, Girard PA, Kunst F, Boemare N, et al. Site-specific antiphagocytic function of the Photorhabdus luminescens type III secretion system during insect colonization. Cell Microbiol. 2005;7(3):363-71.
96. Resko ZJ, Suhi RF, Thota AV, Kroken AR. Evidence for intracellular Pseudomonas aeruginosa. J Bacteriol. 2024;206(5):e0010924.
97. de Souza Santos M, Orth K. Intracellular Vibrio parahaemolyticus escapes the vacuole and establishes a replicative niche in the cytosol of epithelial cells. mBio. 2014;5(5):e01506-14.
98. Guerra RM, Maleno FD, Figueras MJ, Pujol-Bajador I, Fernandez-Bravo A. Potential Pathogenicity of Aeromonas spp. Recovered in River Water, Soil, and Vegetation from a Natural Recreational Area. Pathogens. 2022;11(11).
99. Tessmer MH, Anderson DM, Pickrum AM, Riegert MO, Frank DW. Identification and Verification of Ubiquitin-Activated Bacterial Phospholipases. J Bacteriol. 2019;201(4).
100. Vanderwoude J, Fleming D, Azimi S, Trivedi U, Rumbaugh KP, Diggle SP. The evolution of virulence in Pseudomonas aeruginosa during chronic wound infection. Proc Biol Sci. 2020;287(1937):20202272.
101. Didelot X, Walker AS, Peto TE, Crook DW, Wilson DJ. Within-host evolution of bacterial pathogens. Nat Rev Microbiol. 2016;14(3):150-62.
102. Kurushima J, Kuwae A, Abe A. The type III secreted protein BspR regulates the virulence genes in Bordetella bronchiseptica. PLoS One. 2012;7(6):e38925.
103. Singer HM, Kuhne C, Deditius JA, Hughes KT, Erhardt M. The Salmonella Spi1 virulence regulatory protein HilD directly activates transcription of the flagellar master operon flhDC. J Bacteriol. 2014;196(7):1448-57.